Time Resolution of Silicon Sensors

Werner Riegler, CERN, werner.riegler@cern.ch

February 25, 2022

Vienna Conference on Instrumentation

Abstract

Precision timing with solid state detectors is being employed in many areas of particle physics instrumentation. Applications for pileup rejection and time of flight measurements at the LHC are just two of many notable examples.

During the past years we studied the contributions to the time resolution for various types of silicon sensors. The principal contributors to the time resolution are Landau fluctuations, electronics noise, signal shape fluctuations due to a varying pad response function as well as gain fluctuations.

We discuss silicon pad and silicon pixel sensors, LGAD sensors as well as SPADs and SiPMs. The analytic statistical analysis of the contributions to the time resolution has been performed, resulting in elementary expressions for the timing performance of these sensors. These expressions show the basic directions for optimization of these sensors as well as the fundamental limits to the time resolution.

Planar sensors, 3D sensor, MAPs, LGADs, SPADs

W. Riegler and G. Aglieri Rinella, **Time resolution of silicon pixel sensors**, JINST 12 (2017) P11017

W. Riegler and G. Aglieri Rinella, **Point Charge Potential and Weighting field of a Pixel or Pad in a Plane Condenser**, NIMA 767 (2014) 267-27

W. Riegler, P. Windischhofer, **Time resolution and efficiency of SPADs and SiPMs for photons and charged particles**, NIMA 1003 (2021) 165265

P. Windischhofer, W. Riegler, **The statistics of electron–hole avalanches**, NIMA 1003 (2021) 165327

W. Blum, W. Riegler, L. Rolandi, **Particle Detection with Drift Chambers**,
Springer 2008, ISBN: 978-3-540-76683-4
→ Signal Processing, Noise, optimum filters etc

CERN detector seminar:
https://indico.cern.ch/event/1083146/

Intrinsic time resolution of a silicon sensor

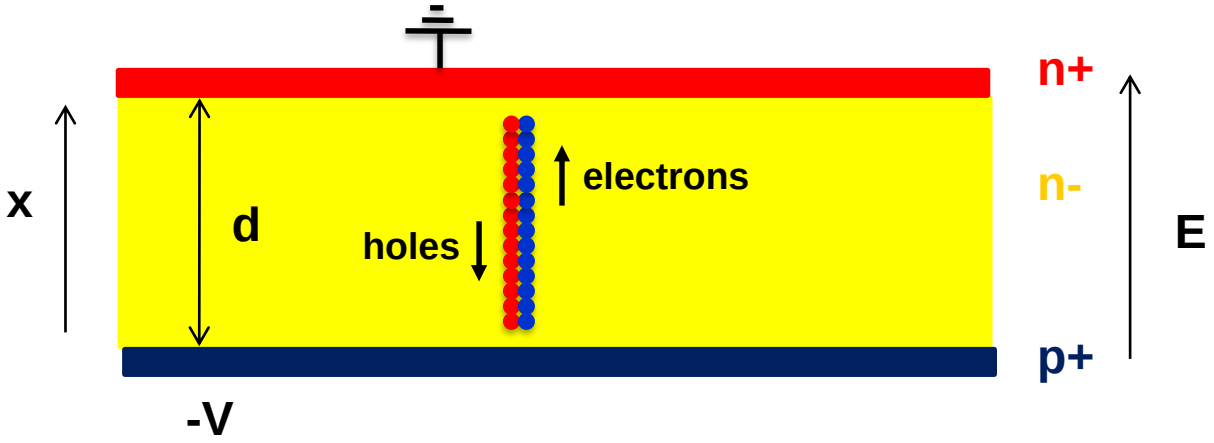

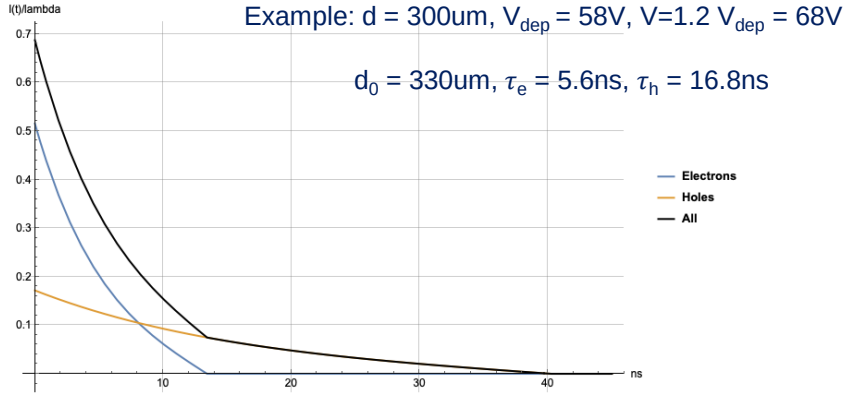

In silicon sensors the signal edge is instantaneous (i.e. sub ps level)

- acceleration of electrons to 10^7cm/s in vacuum is 0.14ps
- passage of the particle through a 50um sensor takes 0.16ps

→ The intrinsic time resolution of a silicon sensor is infinite (sub ps).

→ The time resolution in a planar silicon sensors is a question of signal/noise/electronics and specifically the Landau fluctuations within the electronics integration time.

→ Useful concept that is independent of electronics: center of gravity time resolution

Center of gravity time resolution

Electronics processing of a detector signal

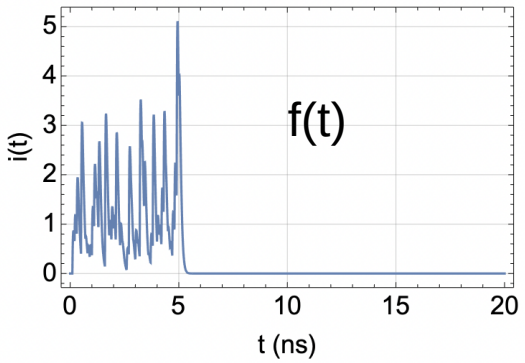

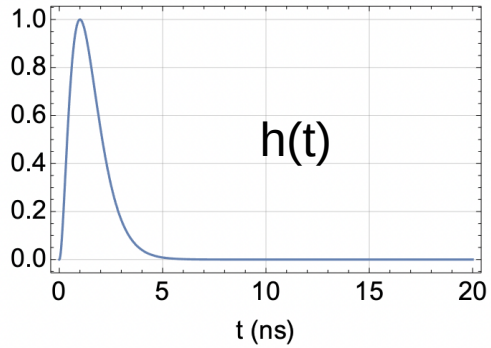

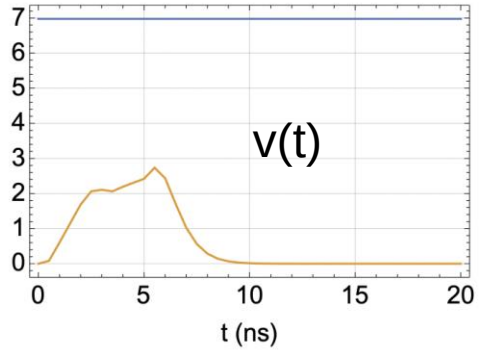

Frontend delta response:

$$h(t) = \left(\frac{t}{t_p}\right)^n e^{n(1-t/t_p)}\,\Theta(t)$$

$$\Theta(t) = \begin{cases} 0 & x < 0 \\ 1 & x > 0 \end{cases}$$

$$\omega_{bw} = n\sqrt{2^{1/(n+1)} - 1}/t_p$$

$$\approx 1.54/t_p \text{ for } n = 4$$

Corresponding transfer function:

$$H(\omega) = \frac{t_p e^n n!}{(n + i\omega t_p)^{n+1}}$$

t_p=1ns f_{bw} ~250MHz

$$v(t) = \int_0^t h(t-t')f(t')dt'$$

-20 log |H(ω)|/|H(0)|

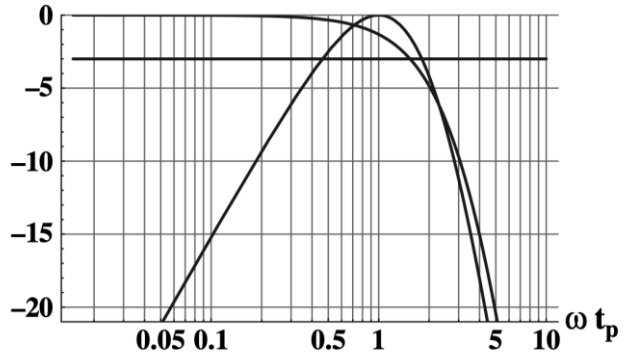

Electronics processing of a detector signal

f(t)

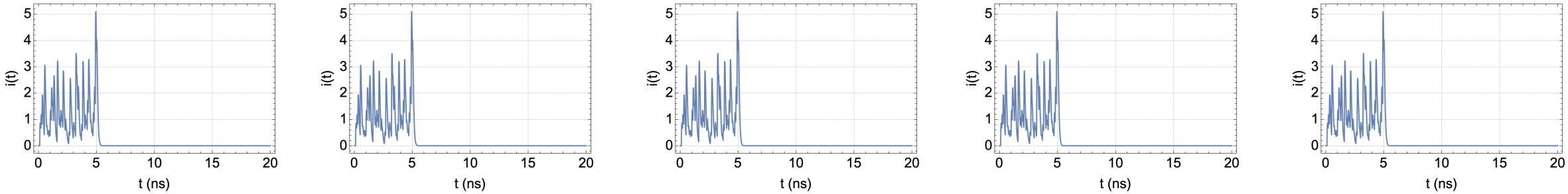

h(t)

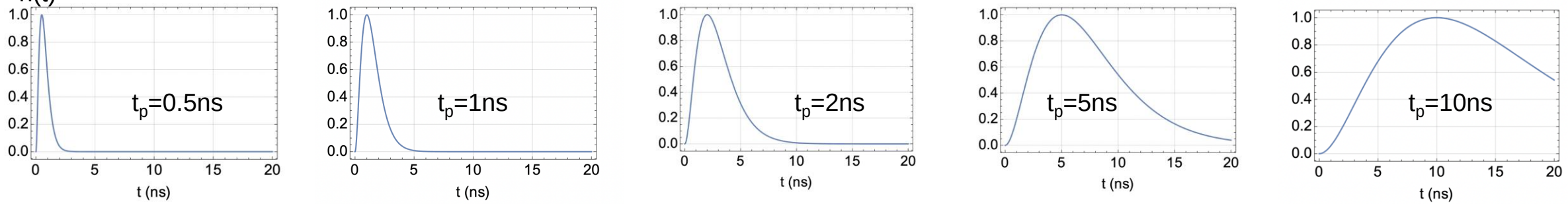

v(t)

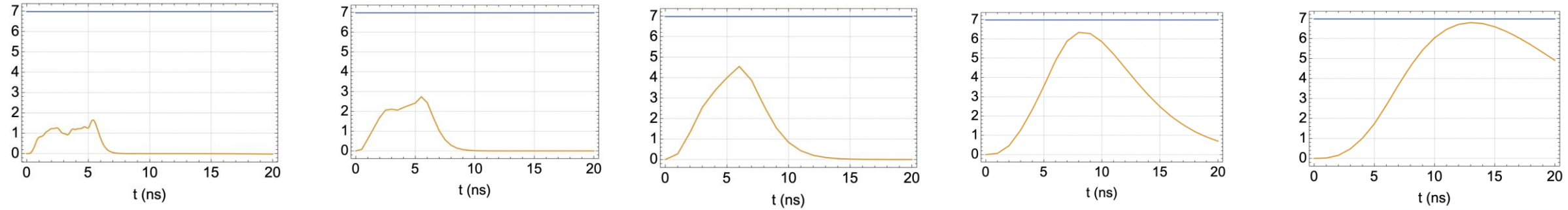

If the peaking time t_p becomes larger than the signal length, the peak of the output signal approaches the total charge. What else … ?

Electronics processing of a detector signal

Signal duration of T i.e. f(t) = 0 for t>T

Electronics peaking time t_p >> T

We are interested in times t>T

$$
\begin{aligned}
v(t) &= \int_0^t h(t-t')f(t')dt' \\
&\approx \int_0^T \left[h(t) - h'(t)t'\right] f(t')dt' \\
&= h(t)\int_0^T f(t')dt' - h'(t)\int_0^T t' f(t')dt' \\
&= \int_0^T f(t')dt' \left[h(t) - h'(t)\frac{\int_0^T t' f(t')dt'}{\int_0^T f(t')dt'}\right] \\
&= q\,\left[h(t) - h'(t)t_{cog}\right] \\
&= q\,h(t-t_{cog})
\end{aligned}
$$

In case the electronics peaking time t_p is longer than the signal duration T, the electronics output signal has

- the same shape as the delta response
- a pulse-height equal to the total charge of the signal
- a 'time displacement' of this delta response by the center of gravity time t_{cog} of the signal.

→ An amplifier that is 'slower' than the signal measures the center of gravity time of the signal

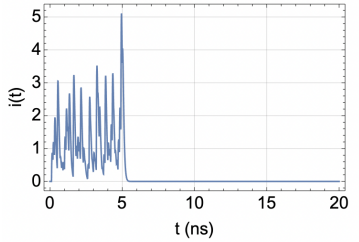

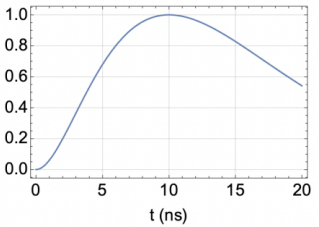

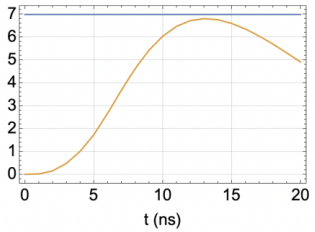

$$
q = \int_0^T f(t')dt' \qquad t_{cog} = \frac{\int_0^T t' f(t')dt'}{\int_0^T f(t')dt'} = \frac{1}{q}\int_0^T t' f(t')dt'
$$

Electronics ‘slower’ than the detector signal, time slewing

Delta response shifted by t_{cog} and scaled by Q

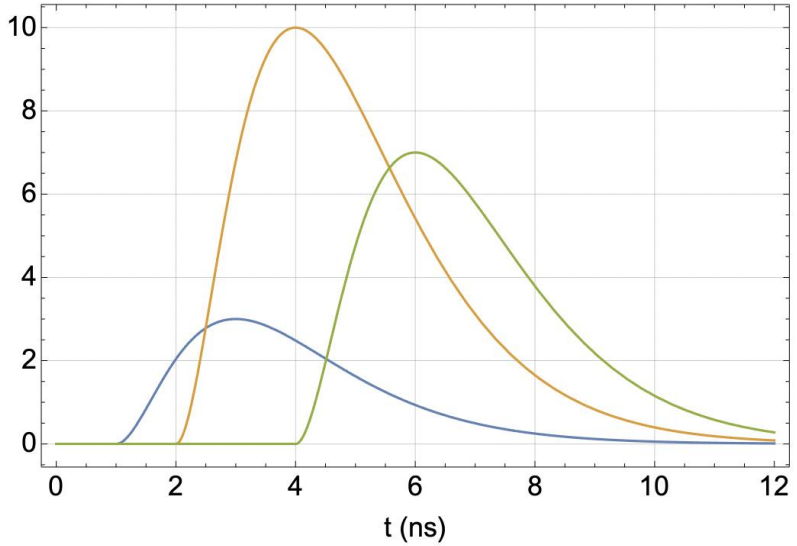

‘time slewing’

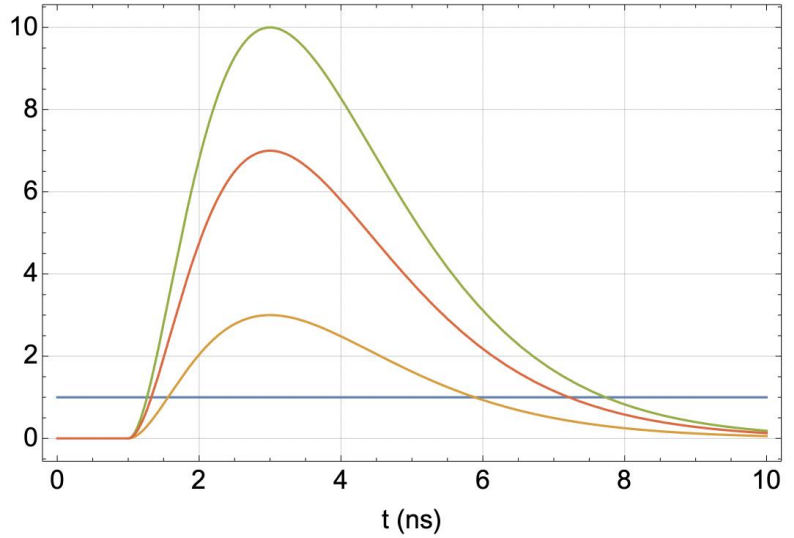

Signal normalized to same amplitude → time

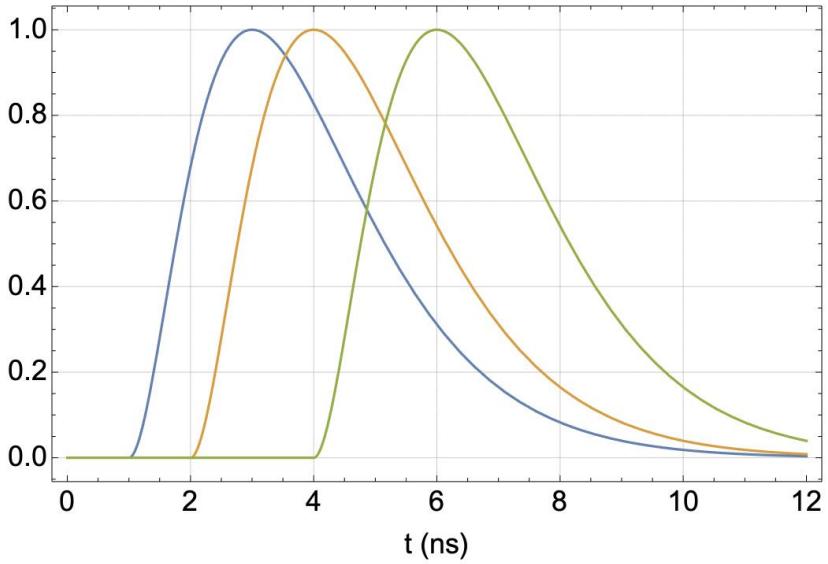

There are many different ways to correct for this slewing effect

- Constant Fraction discrimination
- Standard discrimination using time over threshold to correct for pulse-height
- Standard discrimination + pulseheight to correct for pulse-height
- Standard discrimination + total charge to correct for pulse-height
- Multiple sampling and ‘fitting’ the know signal shape
- ….

→ What is the c.o.g. time resolution of a silicon sensor ?

Time resolution of 3D sensors with ‘trenches’

3D sensor realising a parallel plate geometry, TimeSPOT

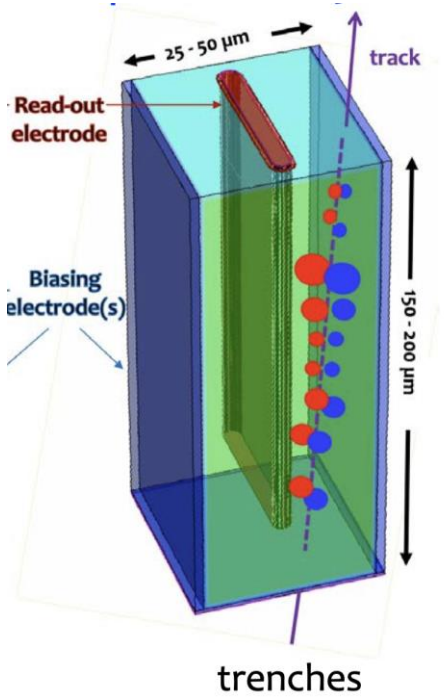

Total charge from the 200um sensor but timing characteristics from a 25um sensor !

L. Anderlini et al., *Intrinsic time resolution of 3D-trench silicon pixels for charged particle detection*. JINST 15, P09029, 2020.

D. Brundu et al., *Accurate modelling of 3D-trench silicon sensor with enhanced timing performance and comparison with test beam measurements*. JINST 16, P09028, 2021.

For a perfectly perpendicular track:
'box' signals from electrons and holes.

Landau fluctuations affect just the total pulse-height, which can be corrected.

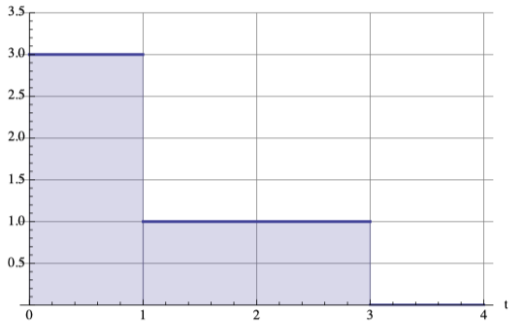

$$i(t) = -\frac{qv_1}{d}\Theta(z/v_1 - t) - \frac{qv_2}{d}\Theta((d-z)/v_2 - t)$$

c.o.g. time of the signal

$$\tau(z) = \frac{1}{2d}\left(\frac{z^2}{v_e} + \frac{(d-z)^2}{v_h}\right)$$

Variance of the c.o.g. Time for uniform distribution of tracks

$$\overline{\tau} = \frac{1}{d}\int_0^d \tau(z)dz \qquad \overline{\tau^2} = \frac{1}{d}\int_0^d \tau(z)^2 dz$$

$$\sigma_\tau = \sqrt{\overline{\tau^2} - \overline{\tau}^2} = \sqrt{\frac{4}{180}\frac{d^2}{v_e^2} - \frac{7}{180}\frac{d^2}{v_e v_h} + \frac{4}{180}\frac{d^2}{v_h^2}}$$

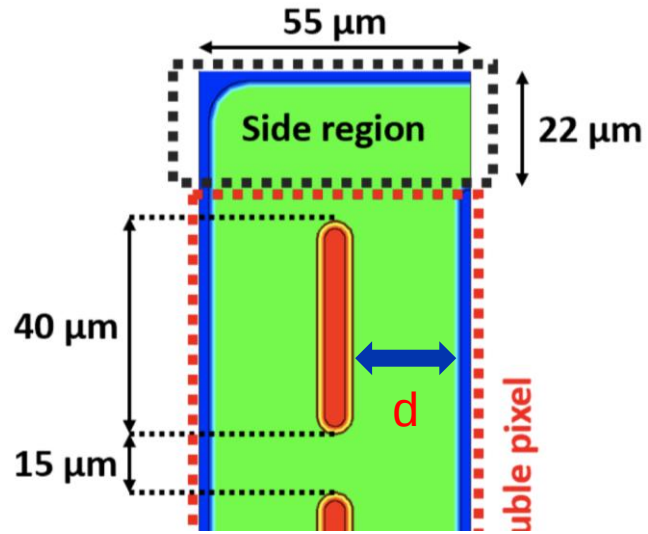

Evaluation of the formula

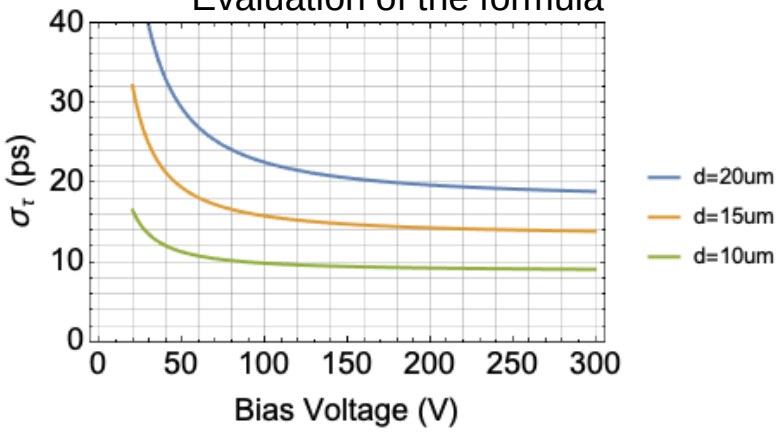

→ 10-20ps achievable and indeed achieved !

Time resolution of planar silicon sensors

Centroid time of a silicon detector signal

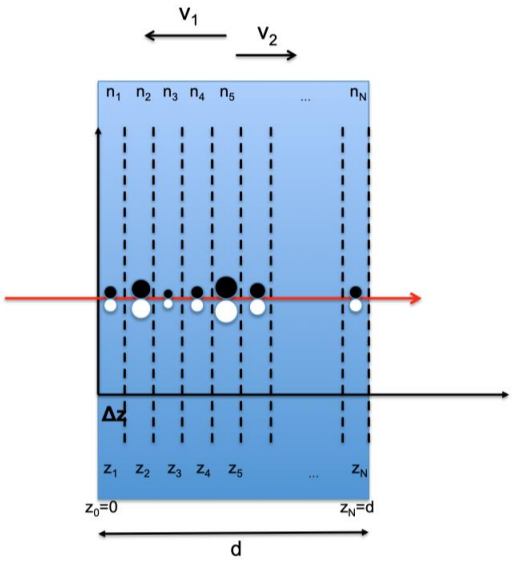

$$\Delta_\tau = w(d)\sqrt{\frac{4}{180}\frac{d^2}{v_1^2} - \frac{7}{180}\frac{d^2}{v_1 v_2} + \frac{4}{180}\frac{d^2}{v_2^2}}$$

$$w(d)^2 = \frac{d}{\lambda}\int_0^\infty \left[\int_0^\infty \frac{n_1^2\, p_{\mathrm{clu}}(n_1)}{(n_1+n)^2} dn_1\right] p(n,d)\,dn$$

For $v_1=v_2$

$$\Delta_t = w(d)\,\frac{1}{\sqrt{180}}\,\frac{d}{v} \approx 0.075\, w(d)\, T$$

50um sensor: 0.075 x 0.2 x 650ps = 10ps

T= total e- drift time = total h drift time
= total width of the 'triangle'

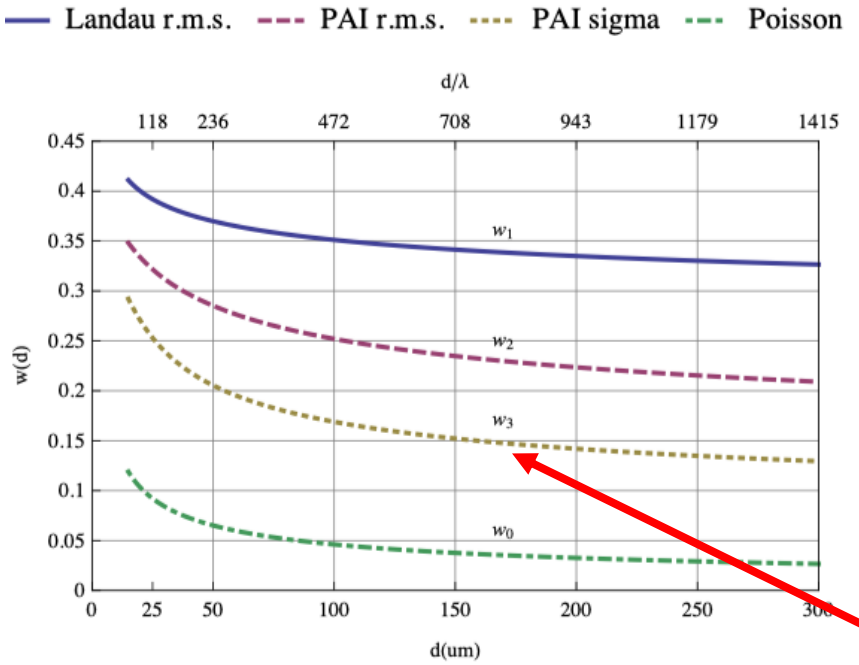

For Si sensors: Important difference between r.m.s. time resolution and the σ of the core of the distribution.

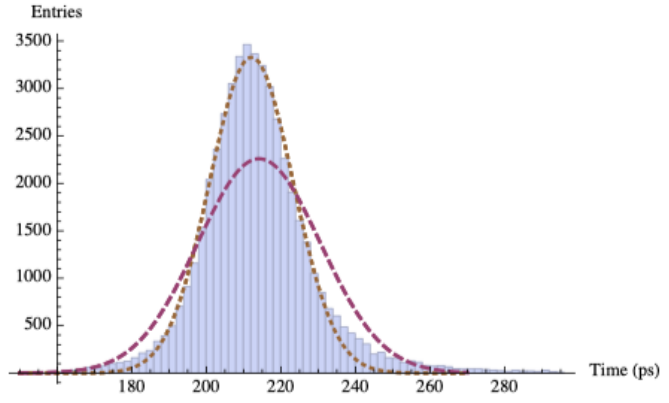

PAI model, Gauss fit

For the Landau Theory

$$w(d)^2 = \frac{1}{\ln(d/\lambda)} \qquad d/\lambda \to \infty$$

For a thinner sensor – the contribution from Landau fluctuation increases.

This worsening of the resolution is superseded by the decrease of e-h drift times.

Leading edge discrimination

$$f(x) = x^n e^{n(1-x)} \tag{4.61}$$

The amplifier output signal is then given by the convolution of the induced signal and the amplifier delta response

$$s(n_1, n_2, \ldots, n_N, x, y, t) = c \int_0^t f\left(\frac{t-t'}{t_p}\right) i(n_1, n_2, \ldots, n_N, x, y, t')dt' \tag{4.62}$$

$$= c\, q \sum_{k=1}^{N} n_k\, g(x, y, k\Delta z, t) \tag{4.63}$$

where $g(x, y, z, t)$ is

$$\begin{aligned} g(x, y, z, t) = {} & \Theta(z - v_1 t) \int_{\frac{z-v_1 t}{d}}^{\frac{z}{d}} f\left(\frac{v_1 t - z + ud}{v_1 t_p}\right) E_w^z(x/d, y/d, u, w_x/d, w_y/d, 1)du \\ & + \Theta(v_1 t - z) \int_0^{\frac{z}{d}} f\left(\frac{v_1 t - z + ud}{v_1 t_p}\right) E_w^z(x/d, y/d, u, w_x/d, w_y/d, 1)du \\ & + \Theta[(d - z) - v_2 t] \int_{\frac{z}{d}}^{\frac{z+v_2 t}{d}} f\left(\frac{v_2 t + z - ud}{v_2 t_p}\right) E_w^z(x/d, y/d, u, w_x/d, w_y/d, 1)du \\ & + \Theta[v_2 t - (d - z)] \int_{\frac{z}{d}}^{1} f\left(\frac{v_2 t + z - ud}{v_2 t_p}\right) E_w^z(x/d, y/d, u, w_x/d, w_y/d, 1)du \end{aligned} \tag{4.64}$$

$$\bar{h}(t) = \frac{c}{w_x w_y} \iint \left[\int_0^1 g(x, y, sd, t)ds\right] dxdy \tag{4.66}$$

and

$$\begin{aligned} \Delta_h^2(t) = {} & w(d)^2 \frac{c^2}{w_x w_y} \iint \left[\int_0^1 g(x, y, sd, t)^2 ds - \left(\int_0^1 g(x, y, sd, t)ds\right)^2\right] dxdy \\ & + \frac{c^2}{w_x w_y} \iint \left(\int_0^1 g(x, y, sd, t)ds\right)^2 dxdy - \left[\frac{c}{w_x w_y} \iint \left(\int_0^1 g(x, y, sd, t)ds\right) dxdy\right]^2 \end{aligned} \tag{4.67}$$

The time resolution is then defined by (figure 18b)

$$\sigma_t = \frac{\Delta_h(t)}{\bar{h}'(t)} \tag{4.68}$$

Here we just discuss the example of an infinitely extended pixel i.e. we use $E_w^z(x, y, z, w_x, w_y, d) = 1/d$, which evaluates $g(x, y, z, t)$ to

$$\begin{aligned} \frac{n^{n+1}}{e^n} \frac{d}{t_p} g(x, y, z, t) = {} & v_1\, \Theta(z - v_1 t)\, [n! - \Gamma(n + 1, t/t_p)] \\ & - v_1\, \Theta(v_1 t - z)\, [\Gamma(n + 1, t/t_p) - \Gamma(n + 1, -(z - v_1 t)/(t_p v_1))] \\ & + v_2\, \Theta((d - z) - v_2 t)\, [n! - \Gamma(n + 1, t/t_p)] \\ & - v_2\, \Theta(v_2 t - (d - z))\, [\Gamma(n + 1, t/t_p) - \Gamma(n + 1, -(d - z - v_2 t)/(t_p v_2))] \end{aligned}$$

50um sensor at 200V for different peaking times and constant fraction discrimination T=0.8ns

c.o.g. time resolution

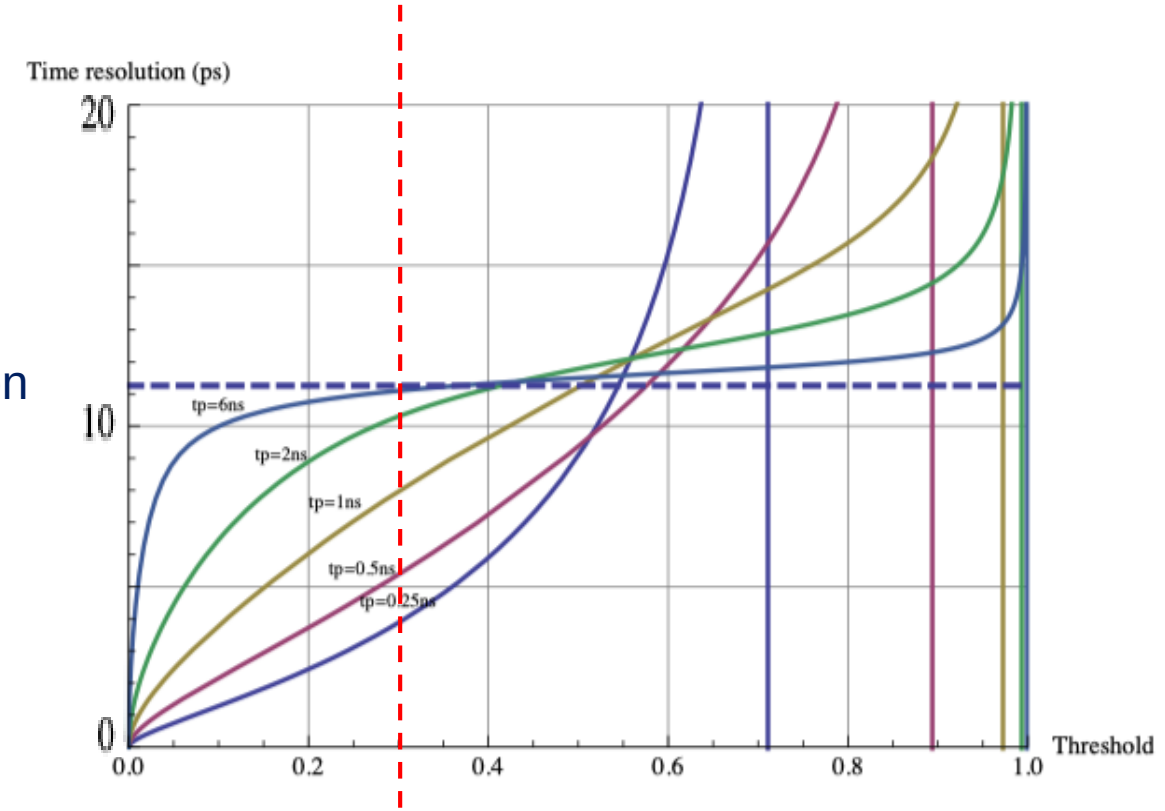

Leading edge discrimination on the signal that is normalized to the total deposited charge.

50um sensor, t_p=0.5ns, threshold at 30% of the charge

→ 5ps time resolution BUT this is unrealistic since S/N becomes too small → Noise will dominate !

Noise

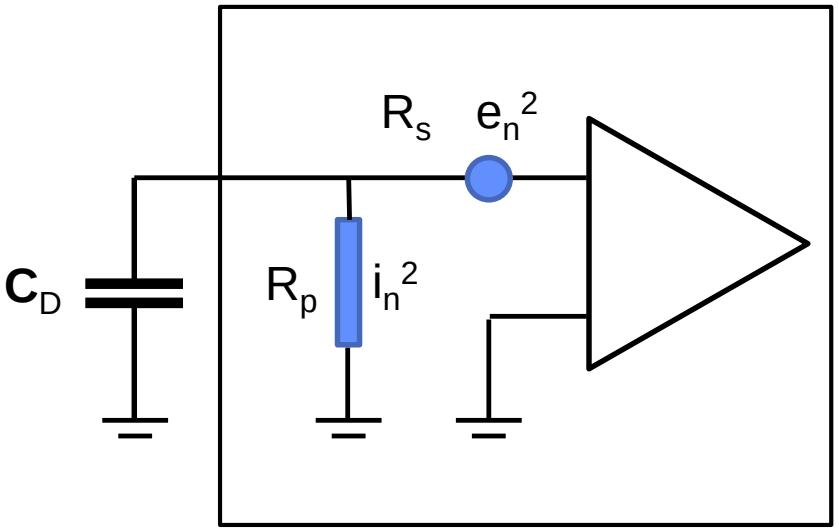

For a sensor that is represented by a capacitance, the noise is determined by the amplifier only. The amplifier noise can be characterized by the parallel and series noise power spectrum.

In case the parallel and series noise power spectra are ‘white’ we can formulate this as noise resistance R_s and R_p.

The level of this noise is a specification of the amplifier, there is no intrinsic noise in the sensor.

This noise level is very specific to the technology, but in general, lower noise requires more power (current through the input transistor etc.).

This places practical limits on the achievable noise level in systems with high granularity i.e. many channels on a small surface.

Optimum filter for best slope to noise ratio

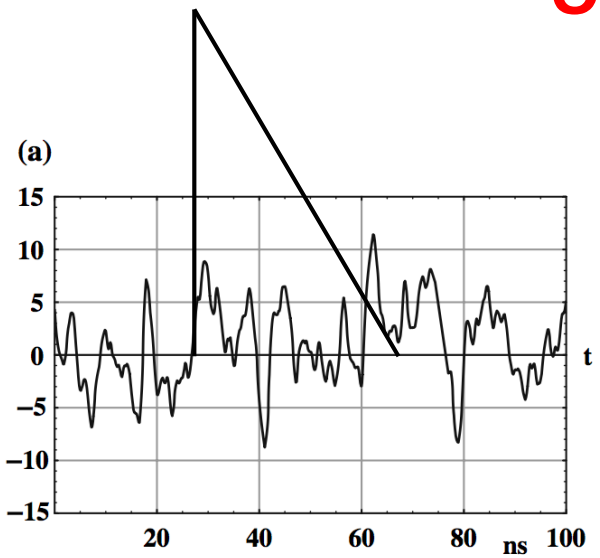

A signal f(t) superimposed to a noise with a noise power spectrum w(ω) is processed by a filter with transfer function H(iω).

$$g(t) = \frac{1}{2\pi}\int_{-\infty}^{\infty} F(i\omega)\,H(i\omega)\,e^{i\omega t}\,d\omega \qquad \sigma^2 = \frac{1}{2\pi}\int_{0}^{\infty} w(\omega)|H(i\omega)|^2\,d\omega.$$

The upper bound for the slope to noise ratio is then

$$\left(\frac{k}{\sigma}\right)^2 \le \frac{2}{\pi}\int_0^{\infty} \frac{|\omega F(i\omega)|^2}{w(\omega)}\,d\omega$$

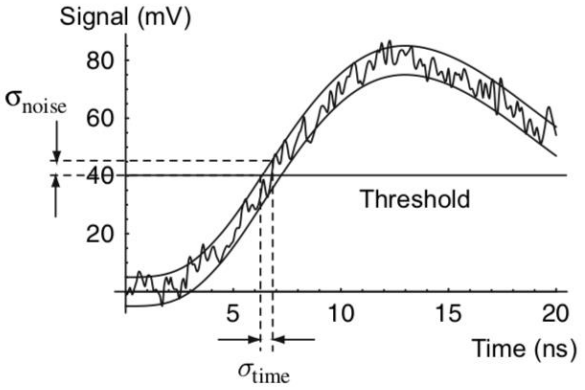

And the optimum transfer function as well as the output signal are

$$H(i\omega) = i\omega\frac{F^*(i\omega)}{w(\omega)}e^{-i\omega t_m} \qquad G(i\omega) = i\omega\frac{|F(i\omega)|^2}{w(\omega)}e^{-it_m\omega}.$$

$$\sigma_{time} = \frac{\sigma_{noise}}{k} \qquad k = \frac{\Delta v}{\Delta t}$$

Optimum filter for best timing

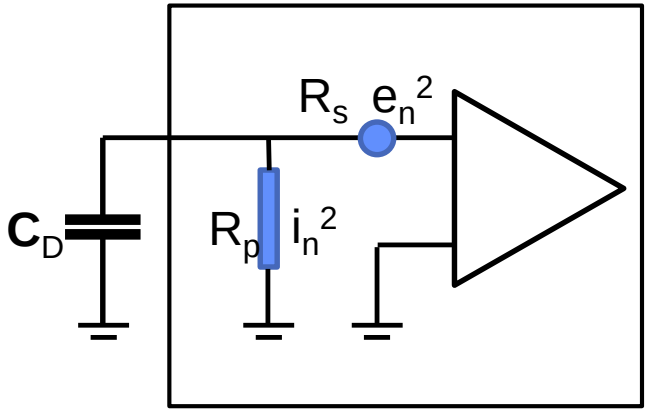

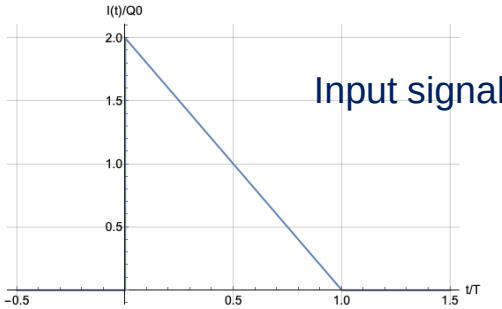

Input signal

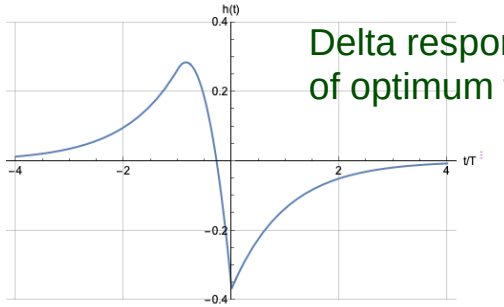

Delta response
of optimum filter

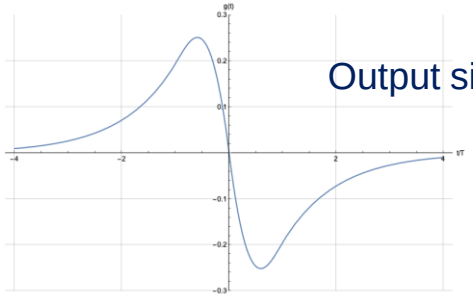

Output signal

Assuming a silicon sensor with negligible depletion voltage and saturated drift-velocity, the signal shape is a triangle:

$$f(t) = \frac{2Q_0}{T}\left(1 - \frac{t}{T}\right) \qquad F(i\omega) = \frac{2Q_0}{\omega^2 T^2}\left(1 - e^{-i\omega T} - i\omega T\right)$$

For the noise we assume series noise and parallel noise together with a detector capacitance C_D

$$w(\omega) = \frac{4kT}{R_p} + 4kTR_sC_D^2\omega^2 = a^2 + b^2\omega^2 \qquad e_n^2(\omega) = 4kTR_s \qquad i_n^2(\omega) = \frac{4kT}{R_p}$$

The maximum slope to noise ratio is

$$\left(\frac{k}{\sigma}\right)^2 \le \frac{4Q_0^2}{a^3T^4}\left(2e^{-aT/b}(b + aT) + \frac{a^2T^2}{b} - 2b\right)$$

If we neglect parallel noise we have

$$\left(\frac{k}{\sigma}\right)^2 \le \frac{8Q_0^2}{3b^2T}$$

This filter is a-causal and can only be approximated in practise.

Realistic preamp transfer function

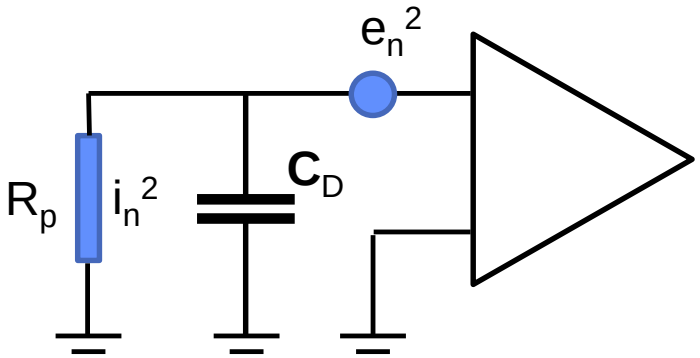

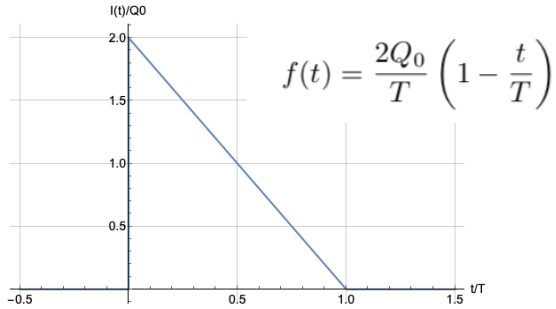

$$f(t) = \frac{2Q_0}{T}\left(1 - \frac{t}{T}\right)$$

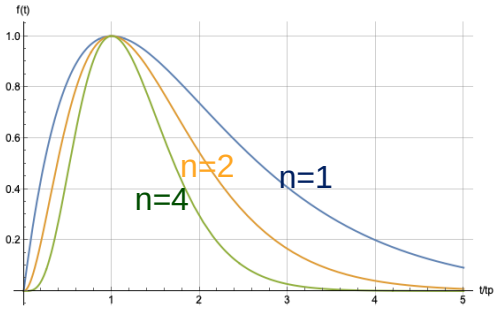

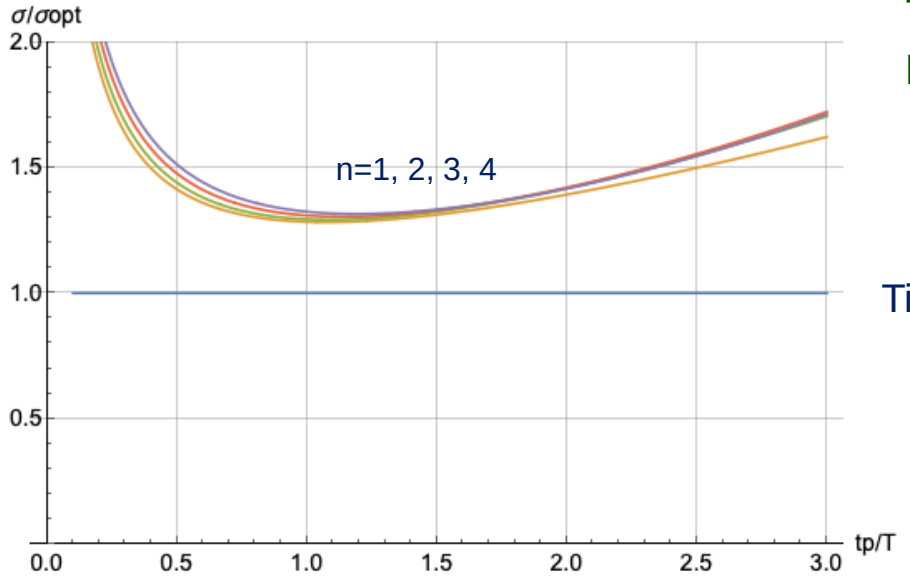

Time resolution for 'standard' preamp delta response.

$$h(t) = e^n n^{-n}\left(\frac{n\,t}{t_p}\right)^n e^{-nt/t_p}$$

Time resolution with optimum filter

Neglecting parallel noise (which is a good approximation in most practical applications) the optimum electronics peaking time t_p is between T and 1.5T.

The achieved time resolution is only about 30% worse than the best achievable one with the optimum filter !

This will give the smallest noise contribution to the time resolution.

Combined effect of Landau fluctuations and noise

If the noise dominates, the optimum peaking time is about t_p ~ 1-1.5T

If the noise is at a similar level to the contribution from Landau fluctuations, the optimum peaking time is still around the same level t_p ~ 1-1.5T and the time resolution is equal to the the c.o.g. time resolution of the silicon sensor.

If the noise is subdominant, shorter peaking times can be improve the time resolution, but with the divergence of the noise contribution at low t_p this will not reach far below the c.o.g. time resolution.

In short: t_p ~ T and $\sigma = \sigma_{c.o.g.} \oplus \sigma_{noise}$ give a good order of magnitude for the achievable time resolution

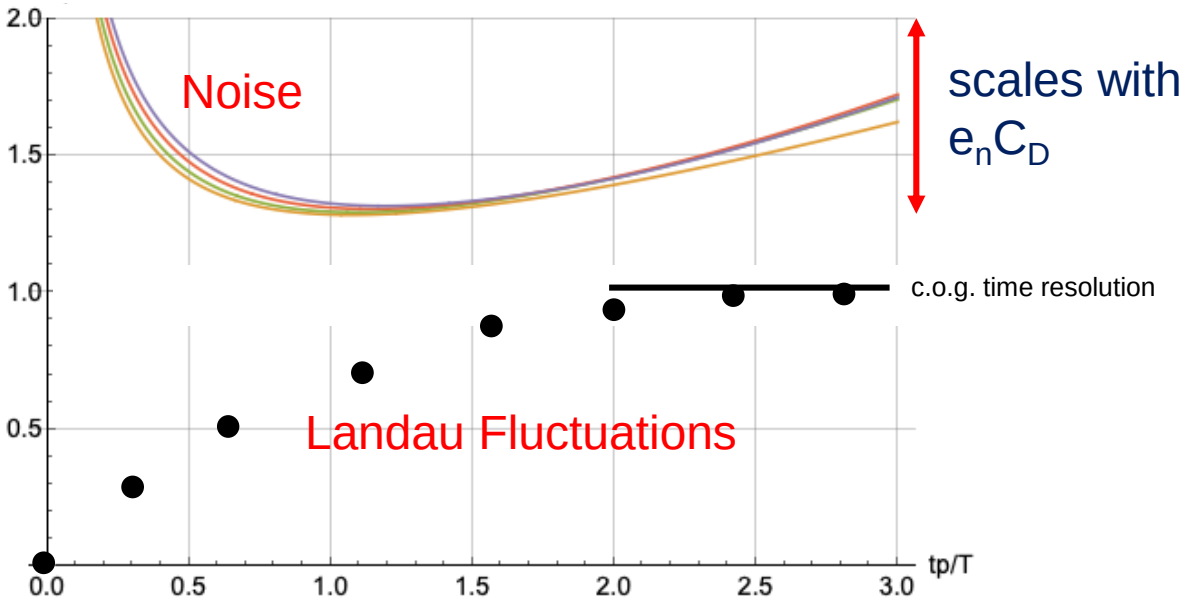

Landau Fluctuations ⊕ Noise

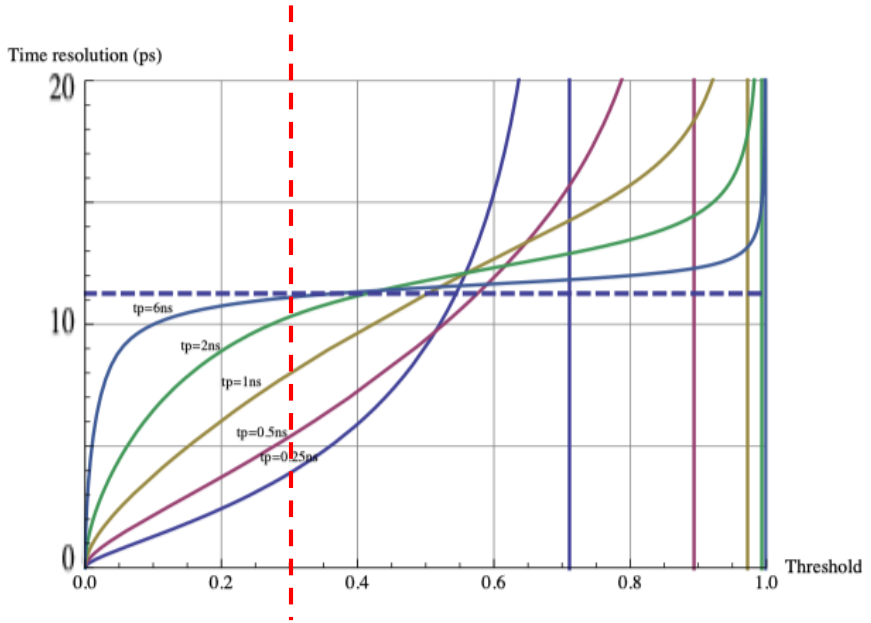

Weighting field effect

Weighting field of a strip in a parallel plate geometry

$$I_a(x,t) = \frac{\lambda v_1}{V_w}\int_0^d E_w(x, z - v_1 t)\Theta(z/v_1 - t)dz$$
$$= \frac{\lambda v_1}{V_w}\left[\psi_1(x,0) - \psi_1(x, d - v_1 t)\right]\Theta(d/v_1 - t)$$

$$I_b(x,t) = \frac{\lambda v_2}{V_w}\int_0^d E_w(x, z + v_2 t)\Theta((d-z)/v_2 - t)dz$$
$$= \frac{\lambda v_2}{V_w}\psi_1(x, v_2 t)\Theta(d/v_2 - t)$$

$$I_1(x,t) = I_a(x,t) + I_b(x,t)$$

Different positions of the particle inside the pixel will lead to different pulse-shapes.

The varying signal shape will lead to variations in the c.o.g. time and therefore affect the time resolution.

This is also called the ‘weighting field effect’.

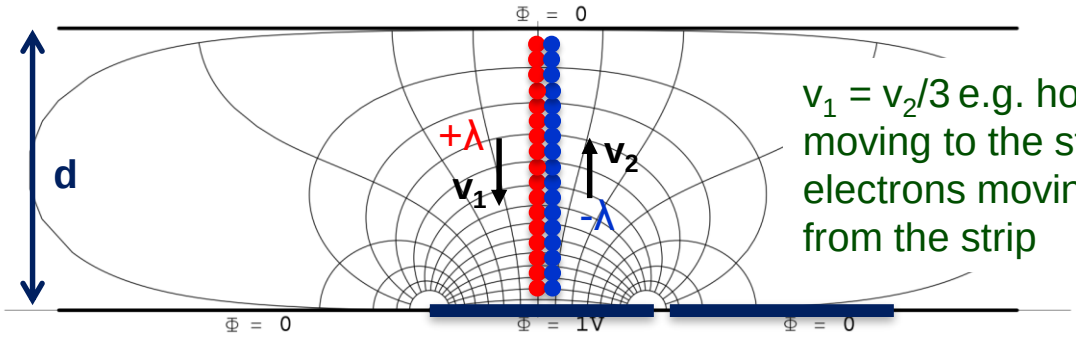

$v_1 = v_2/3$ e.g. holes moving to the strip and electrons moving away from the strip

w>>d

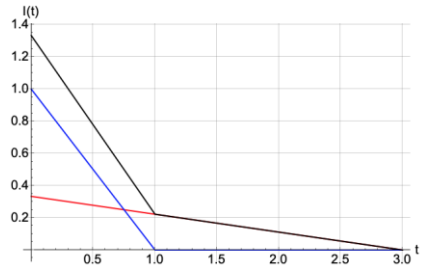

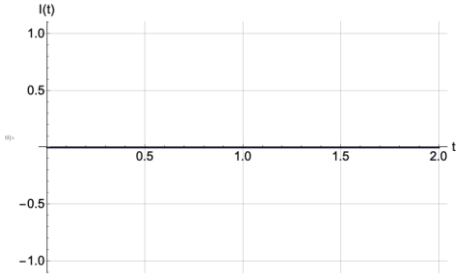

w=d

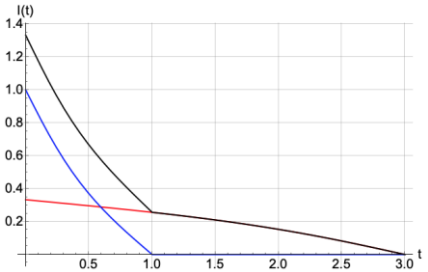

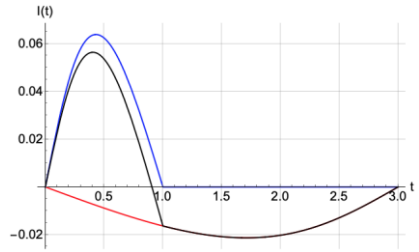

w=d/2

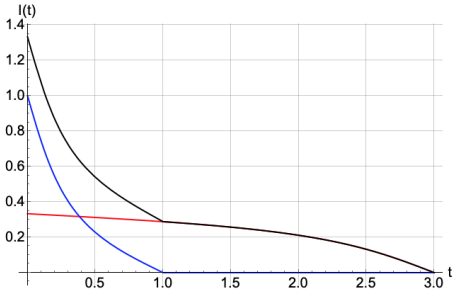

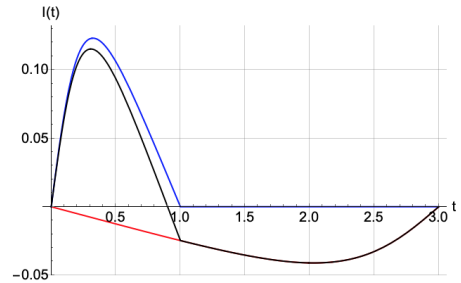

Weighting field fluctuations

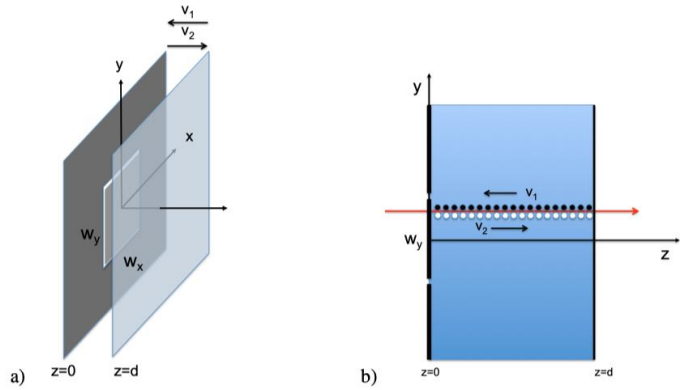

Figure 10. a) A pixel of dimension w_x, w_y centred at $x = y = z = 0$ in a parallel plate geometry of plate distance d. b) Uniform charge deposit of a particle passing the silicon sensor. v_1 is the velocity of charges moving towards the pixel and v_2 is the velocity of charges moving away from the pixel.

Because electrons and holes have different velocities, it makes a significant difference whether the electrons or the holes move to the pixel.

For higher fields (thinner sensors) this difference will decrease.

The dependence on the different parameters is complex.

These fluctuations can dominate the time resolution !

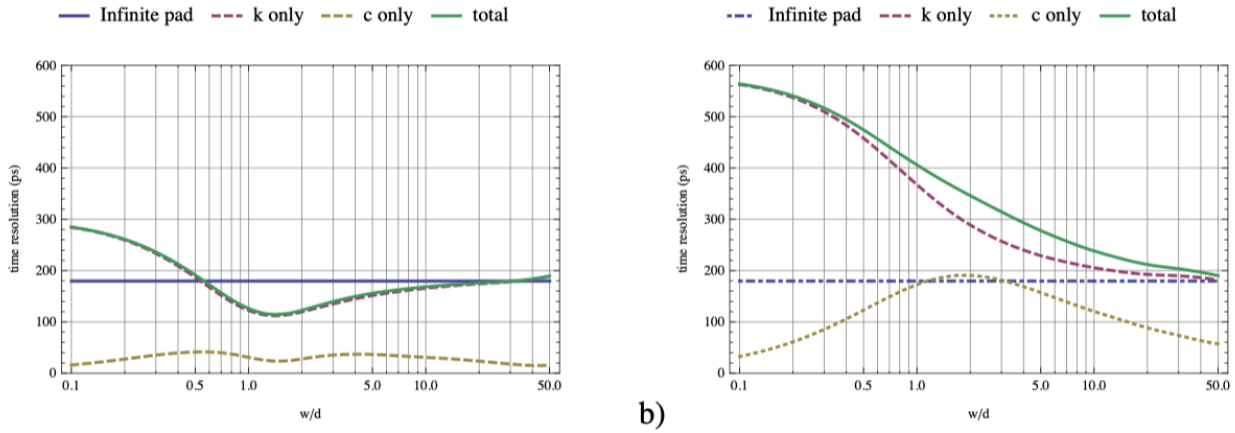

Figure 16. Centroid time resolution for values of $d = 200\ \mu$m and $V = 200$ V as a function of the pixel size w assuming the Landau theory for the charge deposit. The 'c only' curve refers to the effect from a uniform line charge. In a) the electrons move towards the pixel while in b) the holes move towards the pixel.

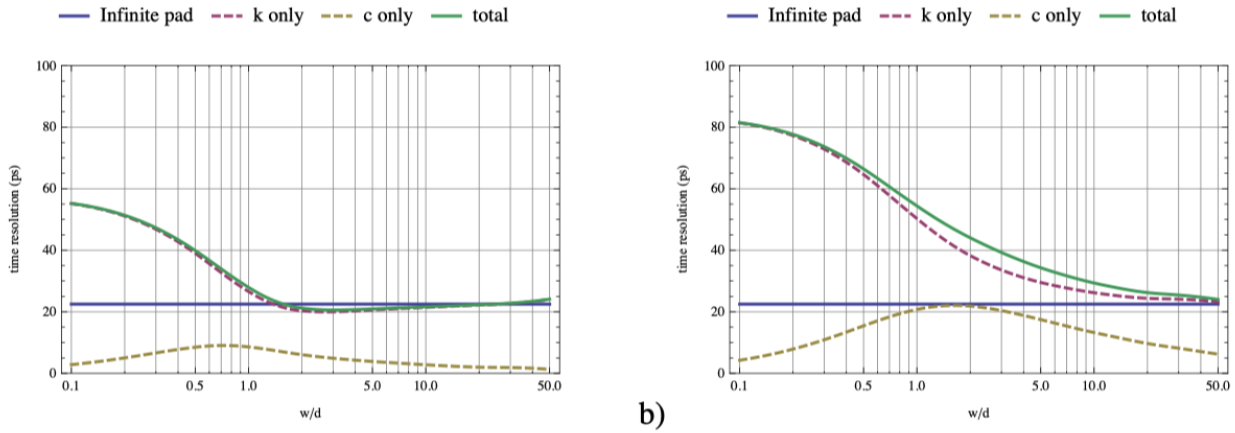

Figure 17. Time resolution for values of $d = 50\ \mu$m and $V = 200$ V as a function of the pixel size w assuming the Landau theory for the charge deposit. The 'c only' curve refers to the effect from a uniform line charge. In a) the electrons move towards the pixel while in b) the holes move towards the pixel.

MAPS time resolution

Time resolution of MAPS with small readout diodes

One flavour of MAPS sensors uses a small ‘collection’ electrode to minimise the capacitance and therefore the noise → E.g. ALPIDE

Since the ‘weighting field’ of the ‘readout electrode’ is concentrated around the diode, the signal consists to a good approximation of a sequence of delta pulses for each electron arriving at the diode.

→ Arrival time distribution.

The time resolution will be somewhere between the arrival time statistics of the first electron and the center of gravity time of all electron arrival times.

The values depend entirely on the geometry and electric field distribution in the sensor and MC simulations are used for evaluation.

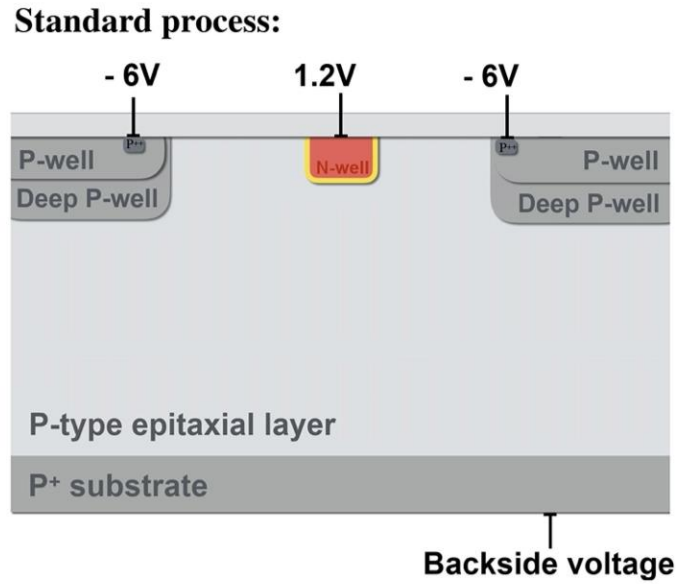

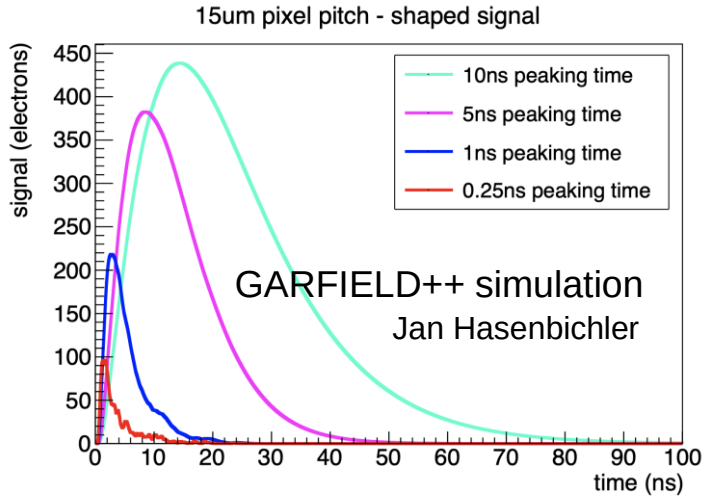

FIGURE 10.1: The simulated shaped signal of one event for the standard flavour with a pixel pitch of 15 µm is shown for peaking times of $\tau = 0.25$ ns, 1 ns, 5 ns and 10 ns.

FASTPIX: a monolithic CMOS Sensor with <200ps timing

Sensor Optimization for FASTPIX

- Hexagonal design reduces the number of neighbors and charge sharing → higher efficiency
- Hexagonal design minimizes the edge regions while maintaining area for circuitry → faster charge collection
- Other optimised parameters include opening of p-wells, size of collection electrode, deep n-implant… to optimise charge collection and capacitance

Simulated hexagonal unit cell – electrostatic potential:

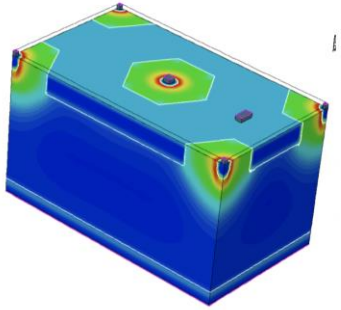

Comparison hexagonal to square pixel cell charge vs. time for particle incident at pixel corner:

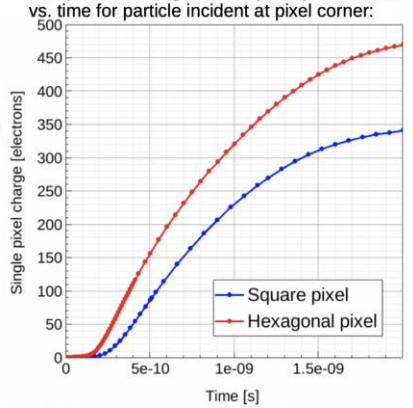

→see M. Munker at iWoRiD 2021 for details on sensor optimisation

- Optimisations important not only for timing, but also for efficiency and radiation tolerance

Test-beam Measurements

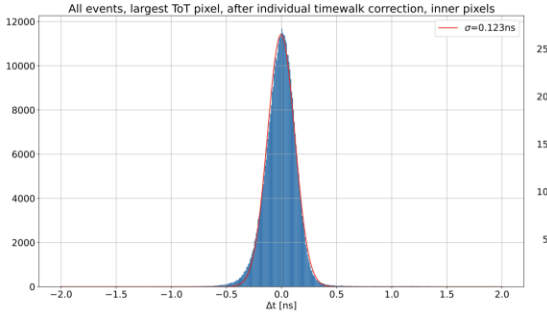

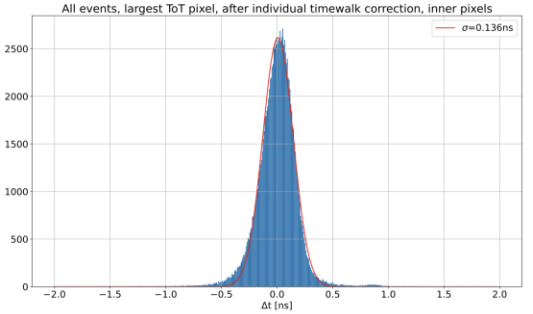

Wafer 18
-6V/-6V pwell/ backside

20x20 µm² matrix (left)
70e threshold

10x10 µm² matrix (right)
50e threshold

- Timing after timewalk correction on 20µm (left) and 10µm (right) matrix
- Pixel-by-pixel correction for best results, reaching below 200ps resolution
- 10µm matrix is operated at lower threshold with a few Hz noise rate
- Larger cluster sizes for 10µm leads to lower average seed charge and thereby more time walk and makes decoding more difficult

< 200ps achieved with a MAPS sensor !

WORKSHOP ON PICO-SECOND TIMING DETECTORS FOR PHYSICS
9–11 Sep 2021
University of Zurich

Eric Buschmann
https://indico.cern.ch/event/861104/contributions/4503032/

Time resolution of LGADs

Avalanche Photo Diode, Low Gain Avalanche Diode

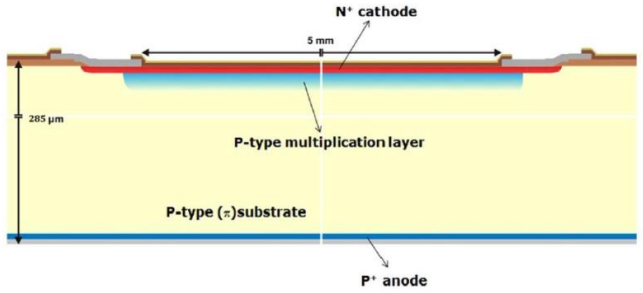

ure 2.2. Cross-section of the core layout of LGAD. A p-type layer is diffused below t

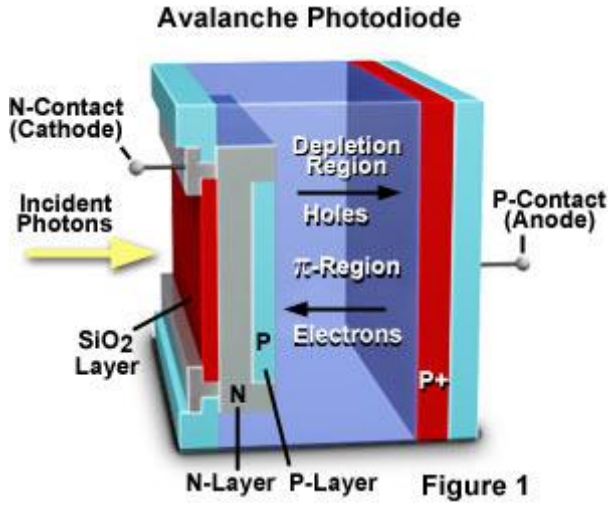

Idea goes back to the 1960ies.

A high field region is implemented in a silicon sensor by doping.

Electrons will produce an avalanche in this high field region.

The high field region is implemented by doping and related 'space-charge' in the volume.

The sensor is operated in a region where there is electron multiplication but not yet hole multiplication.

This allows to have thin sensors (high field, short signal) but still have enough signal charge to overcome the limitation from noise.

For higher fields → electron+hole multiplication → avalanche divergence → quench resistor → SiPM

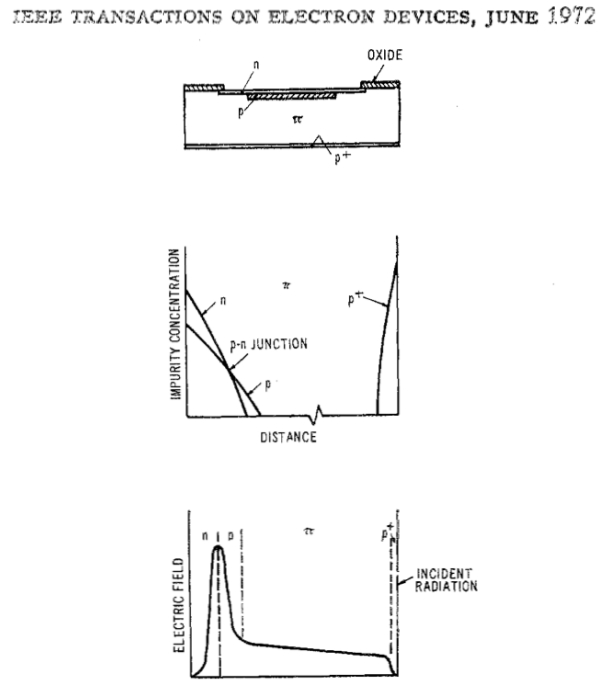

Fig. 1. Sketeches of reach-through avalanche-diode structure, impurity-concentration profile, and electric-field distribution.

Electron (alpha) and hole (beta) multiplication coefficient in silicon

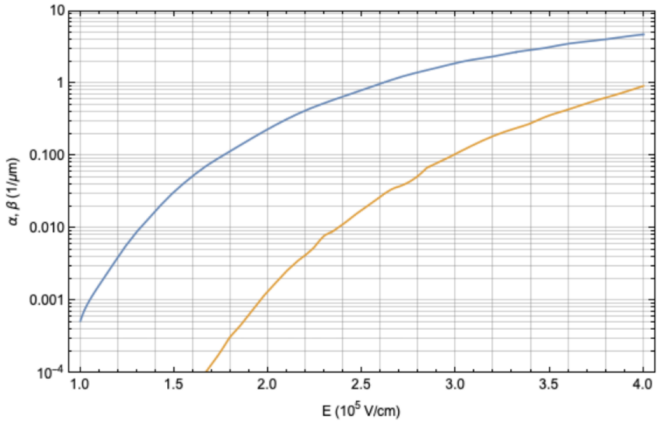

LGAD

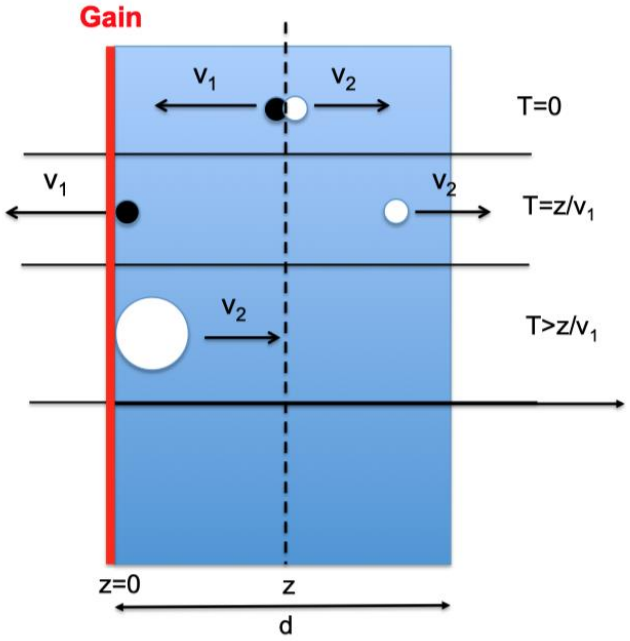

$$w(d)^2 = \frac{d}{\lambda}\int_0^\infty \left[\int_0^\infty \frac{n_1^2\, p_{\mathrm{clu}}(n_1)}{(n_1+n)^2} dn_1\right] p(n,d)dn$$

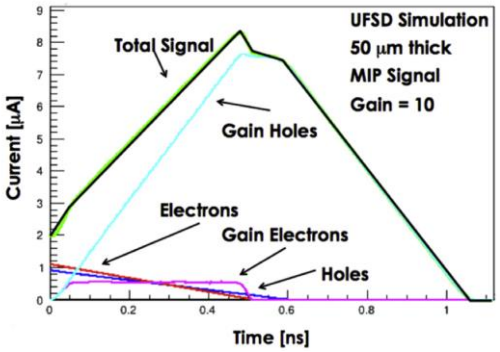

An e-h pair is produced at position z.

The electron arrives at z=0 at time $T=z/v_1$.

The electron multiplies in the high field in the layer at z=0 (infinitely thin).

The holes move back to z=d inducing the dominant part of the signal (all in this approximation).

Centroid time resolution for standard silicon sensor:

$$\Delta_\tau = w(d)\sqrt{\frac{4}{180}\frac{d^2}{v_1^2} - \frac{7}{180}\frac{d^2}{v_1 v_2} + \frac{4}{180}\frac{d^2}{v_2^2}}$$

Centroid time resolution for LGAD

$$\Delta_\tau = w(d)\frac{d}{\sqrt{12}v_1}$$

The signal is now defined by the arrival time distribution of the electrons at the gain layer.

LGAD

LGAD centroid time resolution

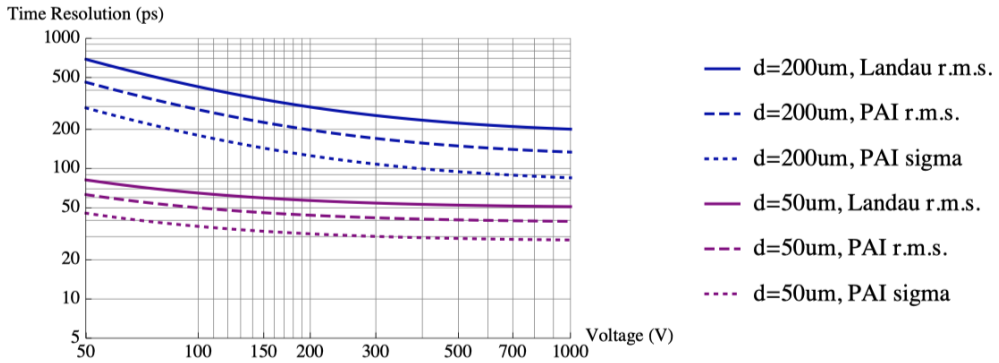

Figure 22. Time resolution for the centroid time from eq. (5.4) for 50, 100, 200, 300μm silicon sensors with internal gain of electrons, assuming a signal only from gain holes. The three curves for each sensor thickness correspond to the Landau theory, the PAI model and a Gaussian fit to the PAI model.

50um sensor at 200V: 30ps

200um sensor at 200V: 140ps

Standard silicon sensor centroid time resolution

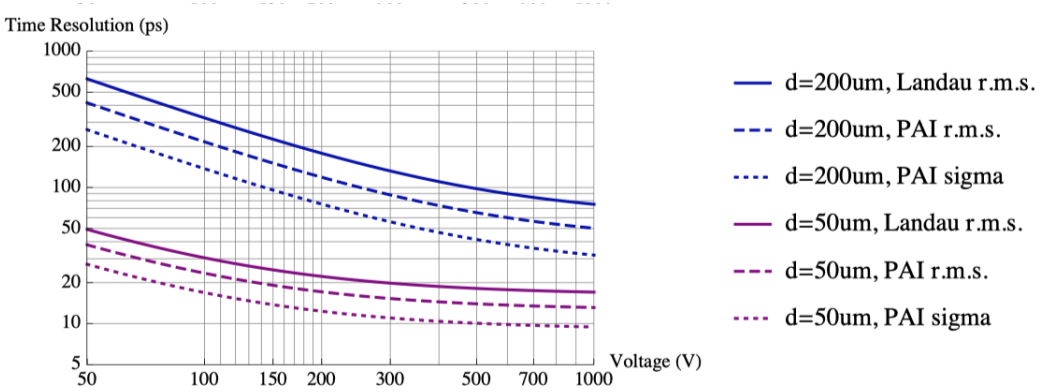

Figure 6. Time resolution from eq. (4.5) for different values of silicon sensor thickness as a function of applied voltage V for the Landau model, the PAI model and a Gaussian fit to the PAI model results.

50um sensor at 200V: 13ps

200um sensor at 200V: 70ps

The c.o.g. time resolution of LGADs is worse than the one for standard silicon sensors due to the very different signal characteristics – essentially an electron arrival time distribution.

Of course – the fact that the signal is larger by a factor 10-15 allows much more relaxed noise requirements, larger pixels etc. …

Time resolution of Single Photon Avalanche Diodes (SPADs)

Single Photon Avalanche Diodes

For very large electric fields, also the holes start to contribute to the avalanche.

α dx = probability for an electron to produce an additional e-h pair along a distance dx

β dx = probability for a hole to produce an additional e-h pair along a distance dx

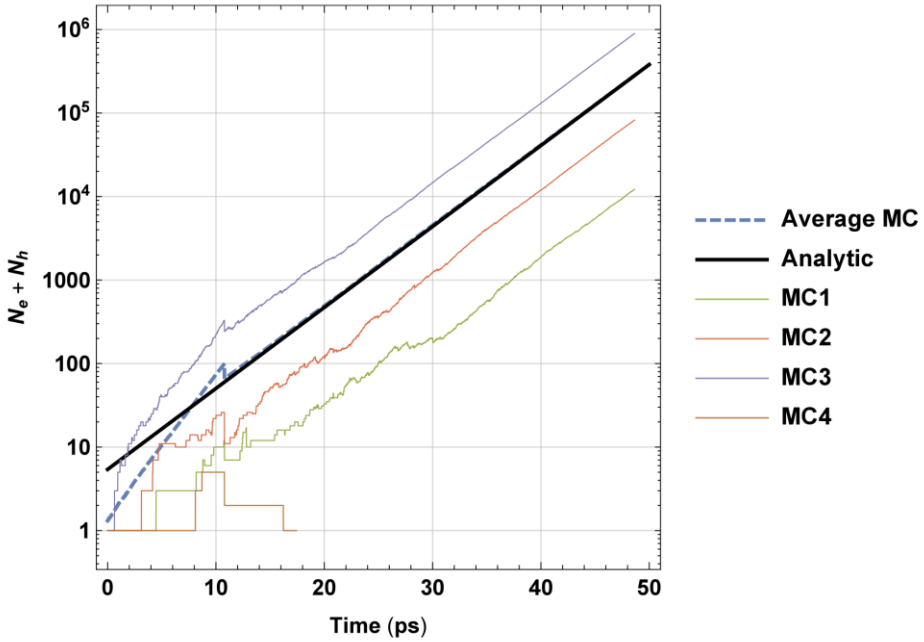

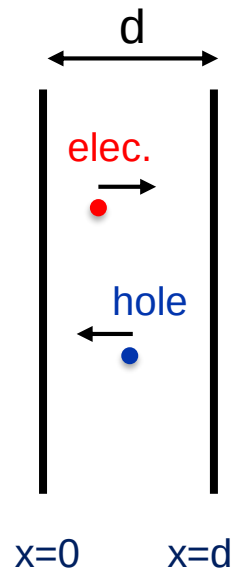

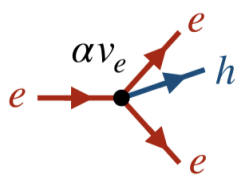

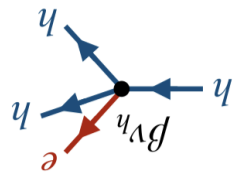

2014 International Conference on Optical MEMS and Nanophotonics

SIMULATION OF ELECTRIC FIELD DISTRIBUTION IN CMOS SINGLE PHOTON AVALANCHE DIODES AT BREAKDOWN VOLTAGE

Jau-Yang Wu and Sheng-Di Lin
Department of Electronics Engineering, National Chiao Tung University, Hsinchu, Taiwan
E-mail: judewu.ee95g@nctu.edu.tw

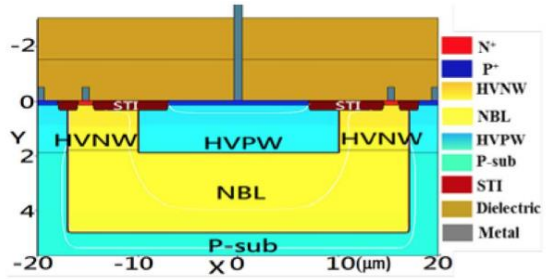

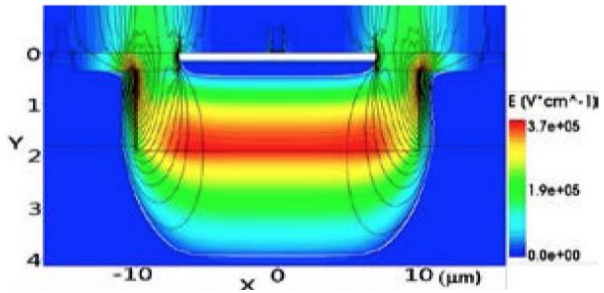

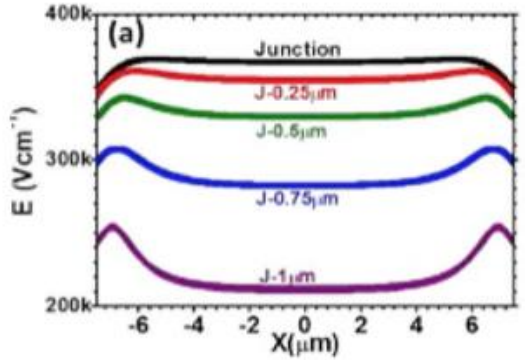

Solution for the average signal

$$n_e(x,t) = \frac{1}{d}\, a(x) \left[n_e^0 u_e(x_0) + n_h^0 u_h(x_0)\right]\ e^{\gamma v^* t}$$

$$n_h(x,t) = \frac{1}{d}\, b(x) \left[n_e^0 u_e(x_0) + n_h^0 u_h(x_0)\right]\ e^{\gamma v^* t}$$

with

$$u_e(x_0) = e^{-a_1 x_0} \sin(k - k x_0/d)$$

$$u_h(x_0) = \frac{e^{-a_1 x_0}}{\alpha d}\left[k\cos\left(k - k x_0/d\right) + \lambda_1 \sin(k - k x_0/d)\right]$$

$$a(x) = \frac{2 v_h k e^{a_1 x} \sin\left(k\frac{x}{d}\right)}{(v_e + v_h)(1+\lambda_1)\sin k}$$

$$b(x) = \frac{2k v_e e^{a_1 x}\left[k\cos\left(k\frac{x}{d}\right) + \lambda_1 \sin\left(k\frac{x}{d}\right)\right]}{(v_e + v_h)\beta d(1+\lambda_1)\sin k}$$

and the constants v^*, a_1, γ, k are defined by

$$v^* = \frac{2 v_e v_h}{v_e + v_h}$$

$$a_1 = \frac{\alpha v_e - \beta v_h}{v_e + v_h} + \frac{v_e - v_h}{v_e + v_h}\frac{1}{d}\ \lambda_1$$

$$\gamma = \frac{\alpha+\beta}{2} + \frac{\lambda_1}{d}$$

$$k = \sqrt{\alpha\beta d^2 - \lambda_1^2}$$

The parameter λ_1 is the largest real solution of the equation

$$\lambda_1 + \sqrt{\alpha\beta d^2 - \lambda_1^2}\cot\sqrt{\alpha\beta d^2 - \lambda_1^2} = 0$$

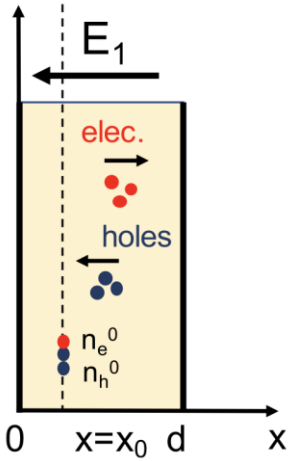

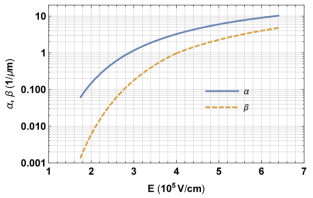

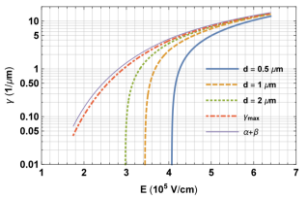

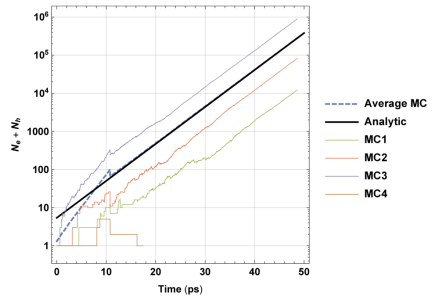

$$\gamma = 0 \qquad \alpha\beta d^2 = \frac{\alpha\beta}{(\alpha-\beta)^2}\ln^2\frac{\beta}{\alpha} \le 1$$

$$\gamma = \frac{\alpha+\beta}{2} - \sqrt{\alpha\beta} \qquad \alpha\beta d^2 = 1$$

$$\gamma = \frac{\alpha+\beta}{2} \qquad \alpha\beta d^2 = \frac{\pi^2}{4} \approx 2.47$$

$$\gamma_{max} = \frac{\alpha+\beta}{2} + \sqrt{\alpha\beta} \qquad \alpha\beta d^2 \to \infty$$

$$N = \int_0^d n(x,t)\,dx$$

$$N_e(t) = B_e\ \left[n_e^0 u_e(x_0) + n_h^0 u_h(x_0)\right]\ e^{\gamma v^* t}$$

$$N_h(t) = B_h\ \left[n_e^0 u_e(x_0) + n_h^0 u_h(x_0)\right]\ e^{\gamma v^* t}$$

where we have

$$B_e = \frac{2k v_h\left[e^{a_1 d}(a_1 d - k\cot k) + k\csc k\right]}{(v_e + v_h)(a_1^2 d^2 + k^2)(1+\lambda_1)}$$

$$B_h = \frac{2k v_e\left[e^{a_1 d}(k^2 + a_1 d\lambda_1 + k(a_1 d - \lambda_1)\cot k) + k(\lambda_1 - a_1 d)\csc k\right]}{(v_e + v_h)\beta d(a_1^2 d^2 + k^2)(1+\lambda_1)}$$

The total induced current becomes

$$I(t) = e_0\frac{E_w}{V_w}\left[v_e N_e(t) + v_h N_h(t)\right]$$

$$= e_0\frac{E_w}{V_w}\left(v_e B_e + v_h B_h\right)\left[n_e^0 u_e(x_0) + n_h^0 u_h(x_0)\right]\ e^{\gamma v^* t}$$

Avalanche fluctuations, SPAD with boundary

Equations for the average electron and hole densities

$$\frac{\partial}{\partial t}\langle n_e(x)\rangle + \frac{\partial}{\partial x} v_e(x)\langle n_e(x)\rangle = \alpha(x)v_e(x)\langle n_e(x)\rangle + \beta(x)v_h(x)\langle n_h(x)\rangle ,$$
$$\frac{\partial}{\partial t}\langle n_h(x)\rangle - \frac{\partial}{\partial x} v_h(x)\langle n_h(x)\rangle = \alpha(x)v_e(x)\langle n_e(x)\rangle + \beta(x)v_h(x)\langle n_h(x)\rangle .$$

Nuclear Inst. and Methods in Physics Research, A 1003 (2021) 165327

The statistics of electron–hole avalanches

P. Windischhofer [a,*], W. Riegler [b]

[a] University of Oxford, United Kingdom
[b] CERN, Switzerland

… surprisingly complex.
Solution gives important insights:

Equations for second moment of the electron and hole densities

$$\begin{aligned}\frac{\partial}{\partial t}\langle n_e(x)n_e(y)\rangle &+ \frac{\partial}{\partial x} v_e(x)\langle n_e(x)n_e(y)\rangle + \frac{\partial}{\partial y} v_e(y)\langle n_e(x)n_e(y)\rangle \\ &= \alpha(x)v_e(x)\delta(x-y)\langle n_e(x)\rangle + \beta(x)v_h(x)\delta(x-y)\langle n_h(y)\rangle \\ &+ \left[\alpha(x)v_e(x) + \alpha(y)v_e(y)\right]\langle n_e(x)n_e(y)\rangle + \beta(y)v_h(y)\langle n_e(x)n_h(y)\rangle \\ &+ \beta(x)v_h(x)\langle n_e(y)n_h(x)\rangle ,\end{aligned}$$

$$\begin{aligned}\frac{\partial}{\partial t}\langle n_h(x)n_h(y)\rangle &- \frac{\partial}{\partial x} v_h(x)\langle n_h(x)n_h(y)\rangle - \frac{\partial}{\partial y} v_h(y)\langle n_h(x)n_h(y)\rangle \\ &= \alpha(x)v_e(x)\delta(x-y)\langle n_e(y)\rangle + \beta(x)v_h(x)\delta(x-y)\langle n_h(y)\rangle \\ &+ \left[\beta(x)v_h(x) + \beta(y)v_h(y)\right]\langle n_h(x)n_h(y)\rangle \\ &+ \alpha(y)v_e(y)\langle n_e(y)n_h(x)\rangle + \alpha(x)v_e(x)\langle n_e(x)n_h(y)\rangle ,\end{aligned}$$

$$\begin{aligned}\frac{\partial}{\partial t}\langle n_e(x)n_h(y)\rangle &+ \frac{\partial}{\partial x} v_e(x)\langle n_e(x)n_h(y)\rangle - \frac{\partial}{\partial y} v_h(y)\langle n_e(x)n_h(y)\rangle \\ &= \alpha(x)v_e(x)\delta(x-y)\langle n_e(y)\rangle + \beta(x)v_h(x)\delta(x-y)\langle n_h(y)\rangle \\ &+ \alpha(y)v_e(y)\langle n_e(x)n_e(y)\rangle + \beta(x)v_h(x)\langle n_h(x)n_h(y)\rangle \\ &+ \left[\alpha(x)v_e(x) + \beta(y)v_h(y)\right]\langle n_e(x)n_h(y)\rangle .\end{aligned}$$

Time resolution of SPAD

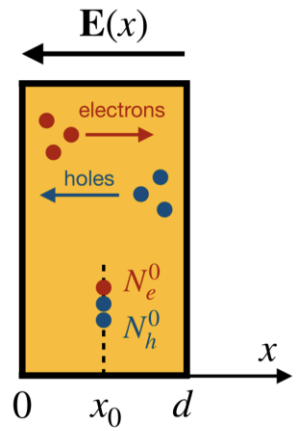

a)

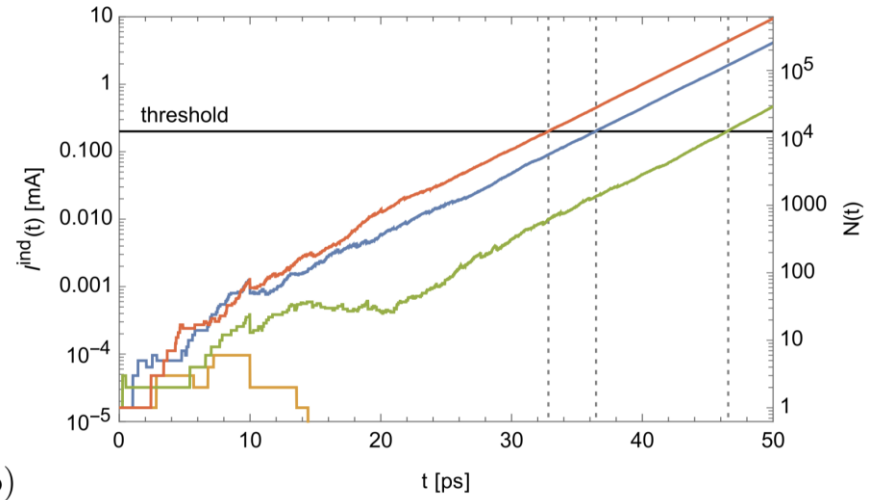

b)

$$I(t) = e_0 \frac{E_w}{V_w} \left[v_e N_e(t) + v_h N_h(t) \right]$$
$$= e_0 \frac{E_w}{V_w} \left(v_e B_e + v_h B_h \right) \left[n_e^0 u_e(x_0) + n_h^0 u_h(x_0) \right] e^{\gamma v^* t}$$

$$\sigma \approx \frac{\sqrt{\psi_1(A)}}{\gamma v^*}$$

$$v^* = \frac{2 v_e v_h}{v_e + v_h}$$

$$A = \frac{n_e^0 \alpha v_e + n_h^0 \beta v_h}{\alpha v_e + \beta v_h}$$

γ determines the exponential growth of the avalanche for long times

$1/\gamma v^*$ determines the time resolution when setting a 'high' threshold to the signal !

The coefficient $\sqrt{\psi_1(A)}$ is O(1) → $1/\gamma v^*$ IS the approximate time resolition of a SPAD

The electron and hole densities become fully correlated over the timescale of $1/\gamma v^*$ i.e. there are no more fluctuations. The fluctuations take place in the very beginning of the avalanches – from there on there is only deterministic grow of the avalanche.

$$C(\lambda_1, \lambda_1, t) \sim C_\infty(\lambda_1, \lambda_1) \left(1 - e^{-\gamma_1 v^* t} \right)$$

Time resolution aSPAD

Approximate r.m.s. SPAD time resolution $1/\gamma v^*$

<10ps is in the cards …

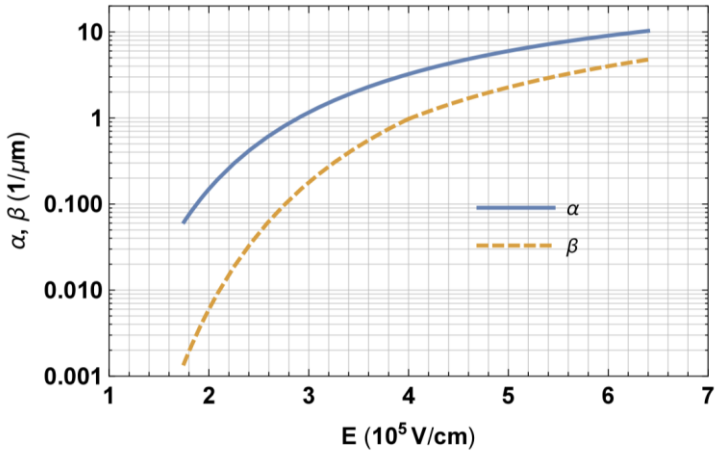

$$v^* = \frac{2v_e v_h}{v_e + v_h}$$

$$\gamma = \frac{\alpha + \beta}{2} + \frac{\lambda_1}{d}$$

The parameter λ_1 is the largest real solution of the equation

$$\lambda_1 + \sqrt{\alpha\beta d^2 - \lambda_1^2}\cot\sqrt{\alpha\beta d^2 - \lambda_1^2} = 0$$

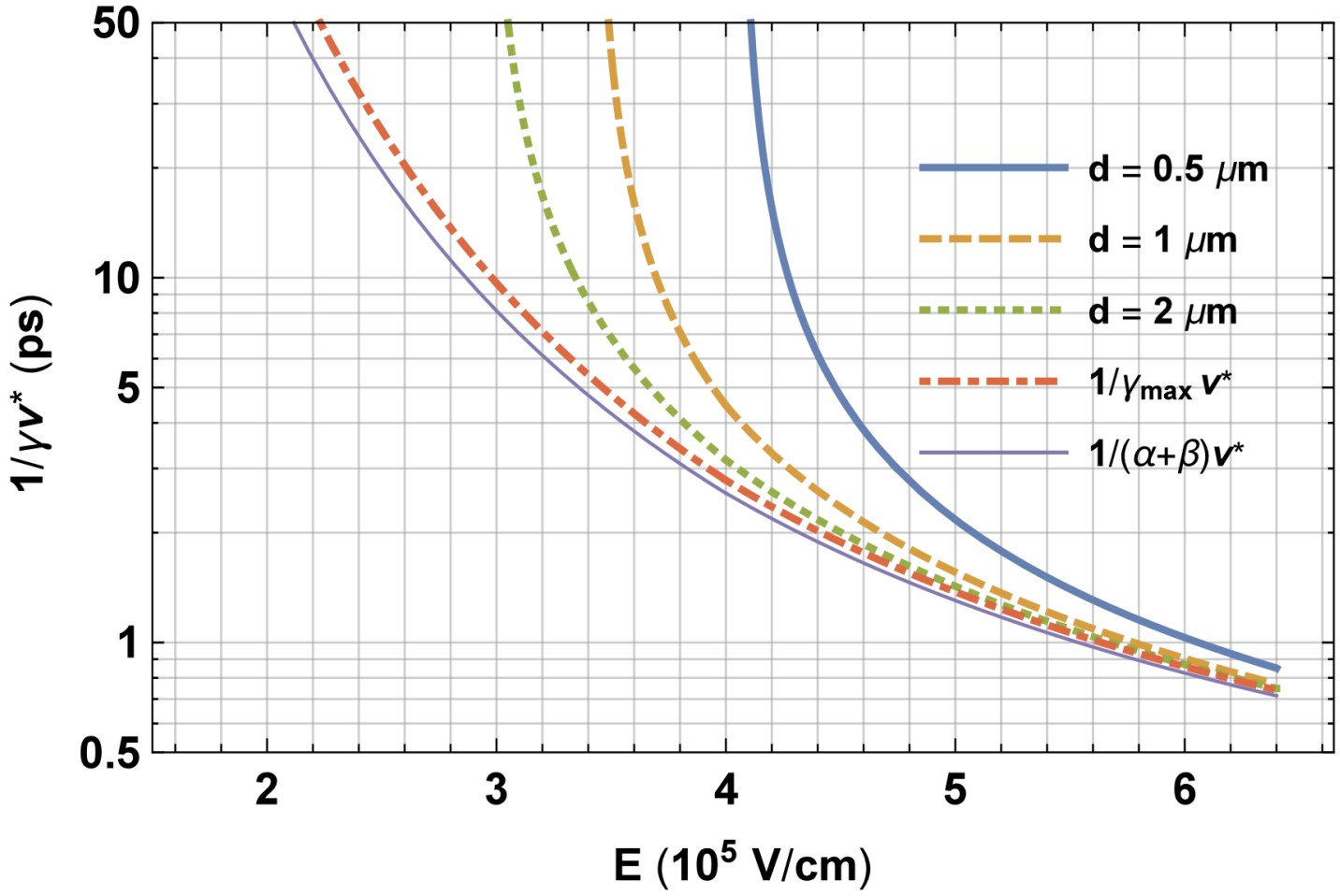

Other contributions to the time resolution of SPADs

Up to now we assumed a given number of electrons and holes at a given position x_0.
→ Only avalanche fluctuations are contributing to the time resolution.

For the measurement of single photons, the conversion point in the gain layer can vary.

For SPADs with a conversion layer, the arrival time distribution of the electrons at the gain layer will contribute.

For the measurement of charged particles, the Landau fluctuations of the charge deposit will contribute to the time resolution.

Conclusion (see paper): for all these scenarios, the time resolution stays around $\sigma = \frac{c_0}{\gamma v^*}$ with c_0 in the order of 1-3.

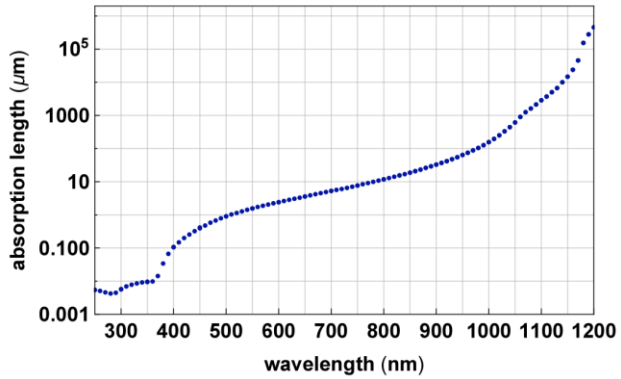

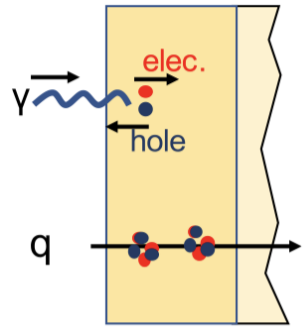

Expect excellent time resolution for MIPs

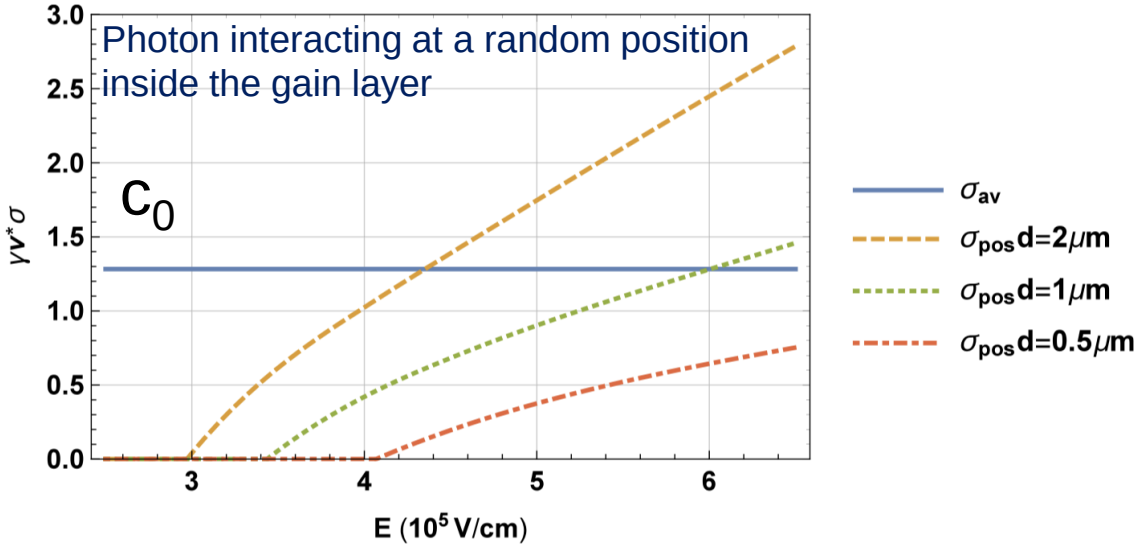

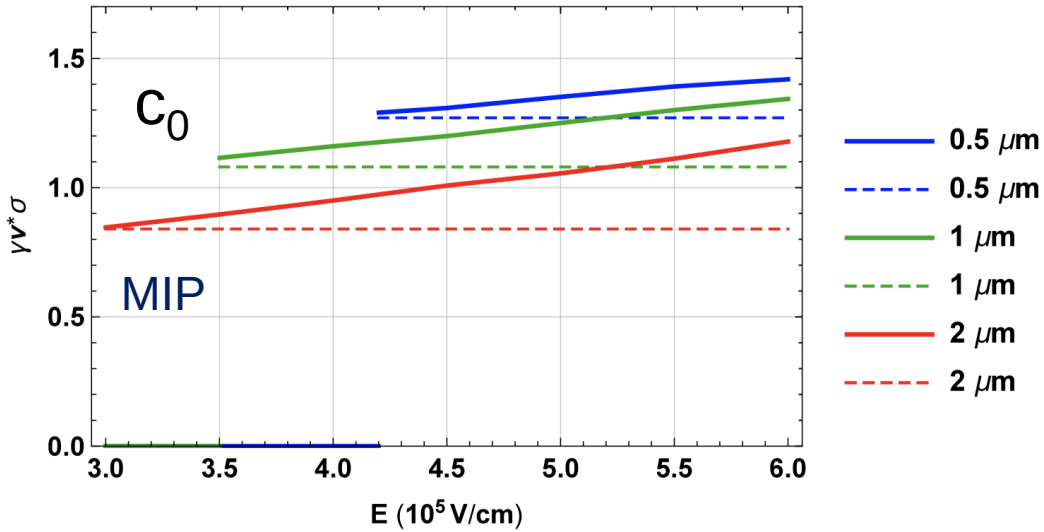

Garfield and Garfield++

CERN | Consult | Writeups | Garfield

Garfield - simulation of gaseous detectors

Responsible at CERN: Rob Veenhof
Manual Type: User Guide
Version: 9
Author: Rob Veenhof
Reference: W5050

Created: 1 Sep 1984
Last Update: 7 Sep 2010
Verified: 7 Sep 2010
Valid until: further notice
Support Level: High

What Garfield does

Garfield is a computer program for the detailed simulation of two- and three-dimensional drift chambers.

Fields

Originally, the program was written for two-dimensional chambers made of wires and planes, such as drift chambers, TPCs and multiwire counters. For many of these configurations, exact fields are known. This is not the case for three dimensional configurations, not even for seemingly simple arrangements like two crossing wires. Furthermore, dielectric media and complex electrode shapes are difficult to handle with analytic techniques. To handle such increasingly popular detectors, Garfield is interfaced with the neBEM program. Garfield also accepts two and three dimensional field maps computed by finite element programs such as Ansys, Maxwell, Tosca, QuickField and FEMLAB as basis for its calculations. The finite element technique can handle nearly arbitrary electrode shapes as well as dielectrics.

Transport and ionisation in gas mixtures

An interface to the Magboltz program is provided for the computation of electron transport properties in nearly arbitrary gas mixtures. Garfield also has an interface with the Heed program to simulate ionisation of gas molecules by particles traversing the chamber.

Transport of particles, including diffusion, avalanches and current induction is treated in three dimensions irrespective of the technique used to compute the fields.

Applications

The program can calculate for instance the following:

- field maps, contour plots and 3-dimensional impressions;
- the wire sag that results from electrostatic and gravitational forces;
- optimum potential settings to achieve various conditions;
- plots of electron and ion drift lines;
- x(t)-relations, drift time tables and arrival time distributions;
- signals induced by charged particles traversing a chamber, taking both electron pulse and ion tail into account.

Related information

- help facility with examples for nearly every command, which can be consulted from within the program and via WWW
- technical notes on specific areas of the program and on related topics
- bug reports
- examples that illustrate the use of the program
- CNL articles (up to 2000)
- news (from March 2005)
- running the program at CERN
- source files of the program

Last updated on 8/2/11.

https://garfield.web.cern.ch/garfield/

TU WIEN

DISSERTATION

Microscopic Simulation of Particle Detectors

ausgeführt zum Zwecke der Erlangung des akademischen Grades eines
Doktors der technischen Wissenschaften unter der Leitung von

Univ. Prof. Dipl.-Ing. Dr. Christian Fabjan
E 141
Atominstitut der österreichischen Universitäten

eingereicht an der Technischen Universität Wien
Fakultät für Physik

von

Dipl.-Ing. Heinrich Schindler
Matrikel-Nr. 0225800
Mechtlerstr. 17, 2100 Korneuburg

Diese Arbeit wurde unterstützt vom
Österreichischen Bundesministerium für Wissenschaft und Forschung.

Wien, im Oktober 2012

CERN-THESIS-2012-208
13/12/2012

https://cds.cern.ch/record/1500583

Garfield++ User Guide

Version 2020.5

H. Schindler

July 2020

https://garfieldpp.web.cern.ch/garfieldpp/

Summary

We have derived elementary expression for the time resolution in silicon sensors

3D sensors with trenches:

$$\sigma_\tau = \sqrt{\frac{4}{180}\frac{d^2}{v_e^2} - \frac{7}{180}\frac{d^2}{v_e v_h} + \frac{4}{180}\frac{d^2}{v_h^2}}$$

Planar sensors:

$$\sigma_\tau = w(d)\sqrt{\frac{4}{180}\frac{d^2}{v_1^2} - \frac{7}{180}\frac{d^2}{v_1 v_2} + \frac{4}{180}\frac{d^2}{v_2^2}} \qquad w(d)^2 = \frac{d}{\lambda}\int_0^\infty \left[\int_0^\infty \frac{n_1^2\, p_{\mathrm{clu}}(n_1)}{(n_1+n)^2} dn_1\right] p(n,d)dn$$

LGADs:

$$\sigma_\tau = w(d)\frac{d}{\sqrt{12}v_1}$$

SPAD photons:

$$\sigma \approx \frac{\sqrt{\psi_1(A)}}{\gamma v^*} \qquad v^* = \frac{2v_e v_h}{v_e + v_h} \qquad A = \frac{n_e^0 \alpha v_e + n_h^0 \beta v_h}{\alpha v_e + \beta v_h}$$

SPAD MIPs:

$$\sigma = \frac{c_0}{\gamma v^*}$$

c_0 in the order of 1-2

and have developed Garfield++ such that all these sensors can be simulated in all detail.